Geoscience Frontiers 15 (2024) 101872

Contents lists available at ScienceDirect

Geoscience Frontiers

journal homepage: www.elsevier.com/locate/gsf

Research Paper

Large dinosaur egg accumulations and their significance for understanding nesting behaviour

L. Ezquerro [a,b,c,d,*], R. Coimbra [e], B. Bauluz [b], C. Núñez-Lahuerta [b,c,d,f,g], T. Román-Berdiel [h], M. Moreno-Azanza [b,c,d]

[a] Departamento de Geodinámica, Estratigrafía y Paleontología, Facultad de Ciencias Geológicas, Universidad Complutense de Madrid, C/ José Antonio Novais, 12, 28040, Madrid, Spain
[b] Aragosaurus∼-IUCA: Recursos Geológicos y Paleoambientales. Departamento de Ciencias de la Tierra. Facultad de Ciencias, Universidad de Zaragoza, C/Pedro Cerbuna 12, 50009 Zaragoza, Spain
[c] Museu da Lourinha, Lourinha, Portugal
[d] GeoBioTec, Department of Earth Sciences, NOVA School of Science and Technology, Universidade Nova de Lisboa, Caparica, Portugal
[e] GeoBioTec, Departamento de Geociencias, Universidade de Aveiro, Aveiro, Portugal
[f] Insitut Català de Paleoecologia Humana i Evolució Social (IPHES-CERCA), Zona Educacional 4, Campus Sescelades URV (Edifici W3), 43007 Tarragona, Spain
[g] Departament áHistòria i Història de ÍArt, Universitat Rovira i Virgili, Av. Catalunya 35, 43002 Tarragona, Spain
[h] Geotransfer IUCA, Departamento de Ciencias de La Tierra, Facultad de Ciencias, Universidad de Zaragoza, Zaragoza, Spain

ARTICLE INFO

Article history:
Received 16 December 2023
Revised 21 April 2024
Accepted 20 May 2024
Available online 22 May 2024
Handling Editor: Richard Damian Nance

Keywords:
Breeding behaviour
Theropod
Taphonomy
Stable isotopes
Magnetic susceptibility
Jurassic

ABSTRACT

The accurate identification of dinosaur egg accumulations as nests or clutches is crucial for understanding the reproductive behaviour of these extinct species. However, existing methods often rely on the presence of complete eggs and embryo remains, and sedimentological criteria that are only applicable to well-structured sediments. In this study, we introduce an innovative approach to characterize egg accumulations in structureless sediments, where traditional nest structures may not be preserved. Our methodology employs a unique combination of sedimentological, taphonomic, geochemical, and geophysical proxies for the study of egg accumulations. We applied this approach to the egg accumulation from Paimogo (Jurassic, Portugal), traditionally interpreted as a nest. Our findings reveal that the Paimogo egg assemblage is a secondary deposit, resulting from a flooding event in a fluvial plain that dismantled several allosauroid and crocodylomorph clutches. The eggshell vapor conductance results, coupled with sedimentological evidence, suggest that allosauroid dinosaurs buried their eggs in the dry terrain of overbank areas close to a main channel during the breeding season, likely during the dry season to prevent the embryos from drowning. This research underscores the necessity of multidisciplinary approaches in interpreting egg accumulations and offers a novel methodology for studying these accumulations in structureless sediments. Our findings provide new insights into the breeding behaviour and nesting preferences of these extinct organisms, contributing to our understanding of dinosaur ecology.

1. Introduction

The study of dinosaur egg assemblages has faced the challenge of characterizing them as clutches, nests, or abiogenic accumulations (*e.g.,* Horner, 2000; Jackson et al., 2004; Sander et al., 2008; Liang et al., 2009). Typically, well-preserved eggs in close proximity, and with associated embryonic bones, have been considered unambiguous evidence of *in situ* clutches, or even nests if they are associated with a nesting structure and nest arrangement within clutch, such as egg pairing or rings of eggs (*e.g.,* Currie and Eberth, 1993; Horner, 1999; Varricchio et al., 1999; Huh and Zelenitsky, 2002; Buffetaut et al., 2005; Grellet-Tinner et al., 2006; Grellet-Tinner and Fiorelli, 2010; Jackson and Varricchio, 2016; Yang et al., 2019; Hogan and Varricchio, 2023). In general, the preservation in the geologic record of superficial nesting traces, such as mounds, rims, or open excavations, is difficult to assess due to both erosion and the lack of clear sedimentary features, and only a few exceptionally well-preserved nests have been given a realistic characterization (Horner and Makela, 1979; Norell et al., 1995; Dong and Currie, 1996; Varricchio et al., 1999; Chiappe et al., 2004).

* Corresponding author.
E-mail address: lopezque@ucm.es (L. Ezquerro).

https://doi.org/10.1016/j.gsf.2024.101872

A set of essential criteria, such as the presence of significant portions of eggs, articulated juvenile bones, identification of rims and ridges, truncated stratification, and distinct fill between the nesting structure and the surrounding deposits, have progressively come to be accepted in attempts to identify an egg assemblage as a nest or clutch (Varricchio et al., 1999; Chiappe et al., 2004; Vila et al., 2010). These criteria have been established in well-stratified deposits where most of the egg-bearing sediments correspond to muddy or silty materials deposited in floodplain environments (*e.g.,* Pietucowski, 1998; Carpenter, 1999; Grigorescu et al., 2010; Kim et al., 2022). Recognizing nesting structures excavated or placed in fine-grained massive and pedogenized sediments is extremely difficult, especially if the pedogenesis was subsequent to the egg-laying. Some recent works have proposed the use of palaeosol horizons to discriminate between clutches and accumulations, but these also present several limitations related to establishing the pedogenic profile (*e.g.*, Jackson et al., 2015; Basilici et al., 2017; Botfalvai et al., 2017).

Furthermore, other uncertain factors concerning incubation strategies and the incubation period are still under consideration: for example, the use of vegetation or sediment cover in mounds (*e.g.*, Carpenter, 1999; Horner, 2000), active incubation (*e.g.*, Zelenitsky, 2006; Tanaka et al., 2018), and filled holes or exposed trenches (*e.g.,* Vila et al., 2010; Grellet-Tinner et al., 2012; Hechenleitner et al., 2016). Analysis of the eggshell structure can also be used as a criterion in identifying the possible presence of nesting structures. For example, eggshell conductance, which depends on eggshell porosity, is relevant to the incubation strategy, as it controls the diffusion of water vapour and respiratory gases through the eggshell (Deeming, 2006). Eggshells with higher porosity (high conductance) are associated with high humidity and low oxygen conditions, which point to underground development (Seymour, 1979; Tanaka et al., 2015). The presence of ornamentation on the outer surface of the eggshell, and the type of such ornamentation, has also been interpreted as a defence against the plugging of the pores by vegetation and sediment (Sabath, 1991; Grellet-Tinner et al., 2006), although this interpretation may need to be reconsidered according to some authors (Zelenitsky and Therrien, 2008).

Here, we present an innovative approach to the study of egg accumulations in structureless sediments where nesting traces can be obscured. The strengths of this work are the combination of sedimentological, taphonomic, geochemical, and geophysical proxies, some of them never used in the analysis of fossil egg accumulations before. Each proxy corresponds to a specific question to provide a holistic understanding of the egg assemblages and egg-bearing materials, identifying any possible fossil nesting trace or dinosaur-induced modifications. This work has allowed an accurate characterization of an egg accumulation long after the specimen was collected, dealing with the inherent loss of data caused by the preparation of the specimen and its storage over 30 years. The methodology has been successfully applied to the Paimogo egg accumulation, which is characterized by a high number of intact, embryo-bearing eggs closely grouped within < 6 m^2. Further, we present some novel insights into reproductive behaviour, the brooding period, and the incubation strategies of Late Jurassic theropod dinosaurs.

2. Materials and methodology

The study of the Paimogo egg accumulation presented several challenges resulting from the lack of information from the original excavation. The scanty data available are limited to some brief papers such as Mateus et al. (1997, 1998, 2001)), Antunes et al. (1998), and Ricqlès et al. (2001), together with unpublished documents such as Cunha et al. (2004) and some field notes located in Lourinhã Museum. A multidisciplinary approach based on a deep taphonomic study was therefore necessary in order to make up for the shortage of data. Here, we only include a brief summary of each technique used and its purpose. A thorough explanation of the state-of-the-art methods and sampling procedures can be found in Fernandes et al. (2021).

2.1. Stratigraphic and sedimentary analyses

The study of the deposits that was undertaken in order to characterize the sedimentary environment comprised a detailed log of two dm-scale stratigraphic profiles (Vale Pombas Sul and Paimogo Forte) in the studied area and 11 cm-scale sedimentological sections along the blocks in the museum's repository and the outcropping walls close to the palaeontological site. Correlation between blocks and field deposits was based on physical criteria related to bed features such as lithology, texture, strata geometry, and sedimentary structures. The study was augmented by analysis of several thin sections to characterize the structure and texture of the sediments at mm-scale, especially the shape and orientation of the grains, which was established using image analysis provided by ImageJ software following the criteria established in several previous works (*e.g.,* Pueyo Anchuela et al., 2013; Felleti et al., 2016).

In addition, 59 laser grain-size analyses were performed using a laser diffraction particle size analyser at the IPE-CSIC and the University of Zaragoza. The statistical and geometrical distributions of the sizes (*e.g.*, the median, mean, standard deviation, sorting, and skewness) provide quantitative information on the flows, processes, and sedimentary environments (*e.g.,* Syvitski, 1991; Selley, 2000; Brookfield, 2004). Grain-size analyses yield quantitative information when a comparison of the character of sediments deposited in a known environment is required (Nichols, 2009). Curves with the same statistical distribution (mean and standard deviation) are characteristic of the same sedimentary processes (Syvitski, 1991).

Finally, the organic matter content was established in laboratories at the University of Zaragoza through the progressive heating and calcination of 15 samples at temperatures up to 425 °C. The samples were taken both from the blocks and the outcrops to compare the presence of organic matter. The occurrence of vegetation cover to maintain the heat and humidity of the eggs has been hypothesized as playing a significant role in the characteristics of fossil clutches and nests (*e.g.*, Horner, 2000; Jackson et al., 2004; Zelenitsky, 2006).

2.2. Geochemical analysis

We followed Coimbra et al. (2023) with a view to acquiring high-quality geochemical data from the eggshell samples. We refer to this paper for a detailed description of the methods of geochemical sampling, but here we provide a brief description. The external surface of 89 selected eggshells and seven carbonate nodules was drilled using a hand drill with a 1-mm diamond drill. Diagenetic overgrowth on the eggshell surfaces was removed before sampling was undertaken using the same hand drill, which was carefully cleaned after each eggshell had been cleaned and the sample acquired. The obtained powder was analysed in the inductively coupled plasma-atomic emission spectrometer (ICP-AES) at the facilities of the Institute for Geology, Mineralogy and Geophysics (Ruhr University Bochum, Germany). Stable isotope composition (carbon and oxygen) and elemental concentrations of Ca, Mg, Sr, Fe, and Mn provide substantial data on palaeoenvironmental and palaeobiological conditions. Dissolution of 1.5 mg of the powdered sample in 1 mL of 3 M HNO_3 (over 12 h) was followed by further

dilution with 2 mL of distilled water and filtering. The isotope composition of eggshells makes it possible to discriminate between different eggs and also between different diagenetic alterations (*e.g.*, Cheong-Bin et al., 2009; Riera et al., 2013). The same powder samples were also analysed for their carbon and oxygen isotope composition using a Thermo Fisher Scientific Gasbench II carbonate device connected to a ThermoFinnigan MAT 253 Mass Spectrometer.

2.3. Anisotropy of magnetic susceptibility (AMS) analysis

AMS analysis was carried out on 190 standard cylindrical specimens (2.5 cm × 2.1 cm) from 136 samples collected in four distinct sites (blocks and outcrops) with a water-cooled drill and oriented with a magnetic compass. The AMS of each specimen was measured with a KLY-3S Kappabridge magnetic susceptibility meter (AGICO, Czech Republic) at the University of Zaragoza. Furthermore, to characterize the magnetic mineralogy, eight temperature-dependent susceptibility curves (two per site and lithology) were obtained between 40 and 700 °C, using a CS-3 furnace connected to the KLY-3S. The determinations were carried out using Anisoft software (Chadima and Jelinek, 2009) and Cureval software (Chadima and Hrouda, 2009). AMS distributions can be correlated with the particle arrangement of the rock. They are useful for determining sedimentary grain orientation and for ascertaining any differences between blocks and outcrops related to sedimentary processes or dinosaur activity (Supplementary Data Fig. 1).

Anisotropy of magnetic susceptibility (AMS) is dependent on intrinsic magnetic susceptibility and the degree of preferred orientation of the individual magnetic minerals (*e.g.*, Chadima et al., 2006). The technique is based on the measurement of the directional variations of susceptibility (K) in a standard volume of rock when a weak magnetic field (≤1 ηT) is applied in different directions (*e.g.*, Rees et al., 1982; Rochette et al., 1992; Borradaile and Henry, 1997; Cifelli et al., 2009). It can be expressed as a second-rank symmetric tensor and represented as an ellipsoid in which the principal axes correspond to principal susceptibility axes ($K_{max} \geq K_{int} \geq K_{min}$). The ellipsoid's magnitude and strength thus represent the preferred magnetic grain orientation and alignment in the sample (Park et al., 2013). Various parameters relating to orientation and shape emerge to characterize the magnetic fabric of the rock (*e.g.* Jelinek, 1981; Hrouda, 1982; Borradaile and Henry, 1997). These include the corrected degree of anisotropy ($Pj = \exp[2(\eta_1 - \eta_m)^2 + (\eta_2 - \eta_m)^2 + (\eta_3 - \eta_m)^2]^{1/2}$) quantifying the relative strength of the magnetic fabric; the shape parameter ($T = (2\eta_2 - \eta_1 - \eta_3)/(\eta_1 - \eta_3)$) indicating the shape of the magnetic susceptibility ellipsoid (where $\eta_1 = \ln K_{max}$, $\eta_2 = \ln K_{int}$, $\eta_3 = \ln K_{min}$ and $\eta_m = (\eta_1 + \eta_2 + \eta_3)/3$); the magnetic lineation ($L = K_{max}/K_{int}$) characterizing the intensity of the linear-parallel orientation of the magnetic minerals; the magnetic foliation ($F = K_{int}/K_{min}$) indicating the intensity of the planar-parallel orientation of the magnetic minerals in the rocks; and the magnetic matrix grain degree $q = 2(K_{max} - K_{int})/(K_{max} + K_{int} + K_{min})$ relating the intensity of magnetic lineation in the magnetic foliation plane with the intensity of the foliation.

2.4. Eggshell and egg analysis

A taphonomic analysis of the preservation features of each of the eggs in the assemblage was carried out using naked-eye observations of the shape and physical features of the eggs. Additional observations were made using a digital polarizing microscope (Dino lite AM7013MZT) in the Lourinhã Museum labs to establish other aspects, such as reabsorption of the mammillae, erosion or abrasion of the eggshells, or the presence of anomalous or secondary calcite layers. Eggshell fragments were removed from each of the eggs in the assemblage and examined using a Carl Zeis Merlin field emission scanning electron microscope (FESEM) equipped with an energy dispersive spectroscopy detector for x-ray compositional analysis, housed at the Servicios de Apoyo a la Investigación de la Universidad de Zaragoza. Selected samples were thin-sectioned in standard 30-μm thin sections and studied with an Olympus BX53M petrographic microscope equipped with an Olympus DP27 digital camera, housed in the 'Instituto Universitario de Ciencias Ambientales' (IUCA) of the University of Zaragoza.

The physical parameters of the eggshell were measured using digital callipers and by means of SEM pictures measured using the software Image J (Schneider et al., 2012). Pore diameter and pore surface were measured by drawing ellipses adjusted to the

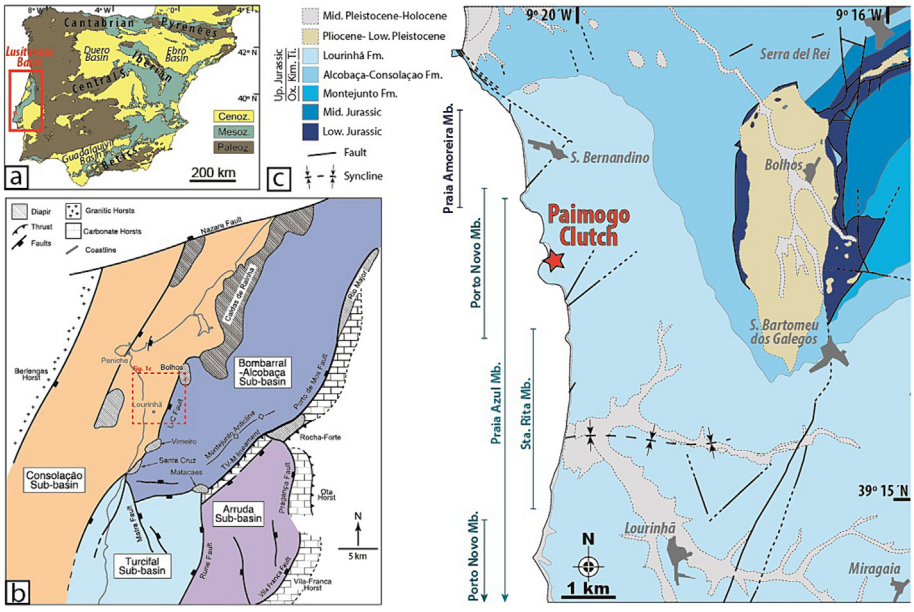

Fig. 1. (a) Location of the Lusitanian Basin in the western Iberian Peninsula. (b) Structural and subbasin division of the study area. (c) Geological map of the Paimogo.

pore section contour, measuring both pore area and mayor axis dimension of the ellipse. The total surface of the eggshell fragment analysed, totalizing 574 mm^2, was measured using a high contrast binary collared picture of the thin sections and, measuring the relative surface occupied by eggshell pixels. Pore diameter and pore abundance were compared from Antunes et al. (1998). Additional parameters were calculated using the formulas compiled by Deeming (2006) and references therein.

Digital replicas of the three main blocks containing eggs were made following the rules established by the International Committee for Architectural Photogrammetry, the so-called 3X3 rules of photogrammetric documentation (Waldhausl and Ogleby, 1994). A series of 168 high-resolution images (overlapping more than 66%) were took with a DSLR camera with a fixed 28-mm lens, manual exposure and low ISO for greater image quality and processed using Agisoft Metashape 1.6. A dense point cloud (52 million points) was used to construct a high-resolution digital elevation model (DEM) (0.198 mm per pixel) with extraordinary coverage (25.6 pt/mm^2). The DEM was the basis for the egg-shape and orientation analysis performed with EllipseFit software (Vollmer, 2018), minimizing the error in measurements and resulting in the statistical distribution of the whole accumulation at once.

3. Geological setting

The Lusitanian Basin is the largest Mesozoic extensional structure at the western Iberian margin (Fig. 1a), limited by the horst of the islands of Berlengas and Farilhões to the west and by the uplifted Variscan Massif to the northeast. The basin was formed as a result of extensional processes related to the North Atlantic spreading, involving four rift phases during the Late Triassic (Triassic-Hettangian), Early Jurassic (Sinemurian–late Oxfordian), Late Jurassic (Kimmeridgian–early Berriasian), and Early Cretaceous (late Berriasian–late Aptian) (Wilson et al., 1989; Rasmussen et al., 1998; Kullberg, 2000). During the first rift phase, the reactivation of NW-SE, NNE-SSW and N-S inherited Variscan faults propagated the deformation towards the continental domain (Wilson et al., 1989; Kullberg, 2000). In the third phase, the rapid subsidence rates together with fault-block rotation and diapirism compartmentalized the structure into distinct sub-basins with differential subsidence (*e.g.,* Leinfelder and Wilson, 1989; Kullberg, 2000; Alves et al., 2002; Carvalho et al., 2005; Taylor et al., 2014).

In the central-western area, four depressions called the Consolaçao, Bombarral-Alcobaça, Arruda and Turifal sub-basins host thick *syn*-rift sedimentary successions (up to 2000 m thick) that comprise marine and continental deposits (Fig. 1b). Due to the complex structure and a certain degree of diachronism, the deposits show some differences between sub-basins. As a result, several nomenclatures and correlations for the stratigraphic units through time have been proposed, summarized in Mateus et al. (2017). Even so, during the late Kimmeridgian, a shift from mixed marine environments (Consolaçao Fm., Abadia Fm., and Alcobaça Fm.) to terrestrial environments (Lourinhã Fm.) occurred more or less rapidly in all the sub-basins, finishing with the establishment of fully continental environments during the Tithonian.

The Paimogo site is located 7 km NW of the village of Lourinhã, consisting of deposits of the Lourinhã Formation (Fig. 1c). The unit is predominantly a fluvial succession, with shallow marine and fluviodeltaic intercalations, and is late Kimmeridgian to late Tithonian in age (Leinfelder and Wilson, 1989; Taylor et al., 2014). According to the division proposed by Hill (1988), the unit comprises five members that replace one another both vertically and laterally. The lowermost Praia de Amoreira Mb. represents a very fine-grained unit, with thick, muddy beds and small channelled sandstone deposits in extensive mudflats. This member grades into the Porto Novo Mb., which is characterized by larger channels and sheet-like sandstones with fewer mudstone beds that correspond to meandering streams and floodplains. The continental facies of the Porto Novo Mb. are interspersed in the Praia Azul Mb. This member comprises lower delta-plain deposits, which exhibit well-organized sandy channels and low-energy muddy beds, including shelly beds of shallow restricted shoreline deposits. The Assenta Mb. contains crevasse and sandy channels interfingered with mudstones and occasional lacustrine and marine deposits. The Assenta Mb. represents the upper delta-plain and fluvial domain of the Praia Azul Mb. Lithologically, the Santa Rita Mb. is much more coarsely grained, with thick gravelly channels of well-rounded clasts in a moderately sinuous meandering system, showing a rapid transition with respect to the Porto Novo and Assenta members.

4. Stratigraphic and sedimentological analysis

4.1. Stratigraphic succession of the Paimogo area

4.1.1. Description

Overall, the studied succession corresponds to a ~ 75 m-thick succession of fine-grained deposits (reddish to greyish silts, mudstones, and marls) that intercalate coarser-grain-sized beds (brownish to greyish sandstones) (Fig. 2a). The correlation of the two sections shows both vertical and lateral changes in the deposits, making it possible to establish four simplified facies associations. The main features of each facies association (lithology, texture, stratal geometry, sedimentary structures) as well as the inferred sedimentary processes and sub-environments are summarized in Table 1.

Mudstones, silts, and marls are the most common lithology in the area and correspond to laterally continuous tabular beds (dm- to m-thick), massive in texture, with occasional laminae appearing in dark-coloured beds. Reddish beds show frequent pedogenic evidence, such as green and yellowish mottles, root traces, and carbonate nodules (both spherical and elongated). Grey strata exhibit scattered root traces and mottling, but nodulization is very common. Irregular, light-coloured sheets (dm-thick), composed predominantly of spherical carbonate nodules (cm-diameter) that coalesce in a calcrete-like bed, appear occasionally interbedded in red mudstones. The sandstones are very coarse to fine in grain size, commonly in fining-upwards sequences, forming thick, well-organized channel bodies (up to 7 m thick) that contain sets of trough and planar cross-bedding, parallel and cross-lamination, and rare ripples; massive levels are rare. Muddy drapes and coal debris are frequent at the bottom; cross-bedding is predominant in the lower and middle parts, whereas burrowing and bioturbation are not infrequent at the top of the brown bodies. Occasionally, there are thin conglomerates with erosive lower and gradational upper contacts, comprising subrounded to rounded pebbles (mostly reworked nodules) in the channel-floor. Well-laminated sets or beds are more frequent in fine-grained sets or beds. The whole succession is highly micaceous, but the grey sandstones and silts contain larger subangular to subrounded biotite and muscovite grains than the muddy beds.

The palaeocurrent pattern for the overall area, mainly consisting of cross-bedding, imbricated pebbles, and scour axes, shows a general trend to S, with two maxima in SSW and SE directions (Fig. 2a). The features of the channelled bodies, together with the palaeocurrent distribution, suggest a low to moderate sinuosity for the channels, consistent with a meandering drainage.

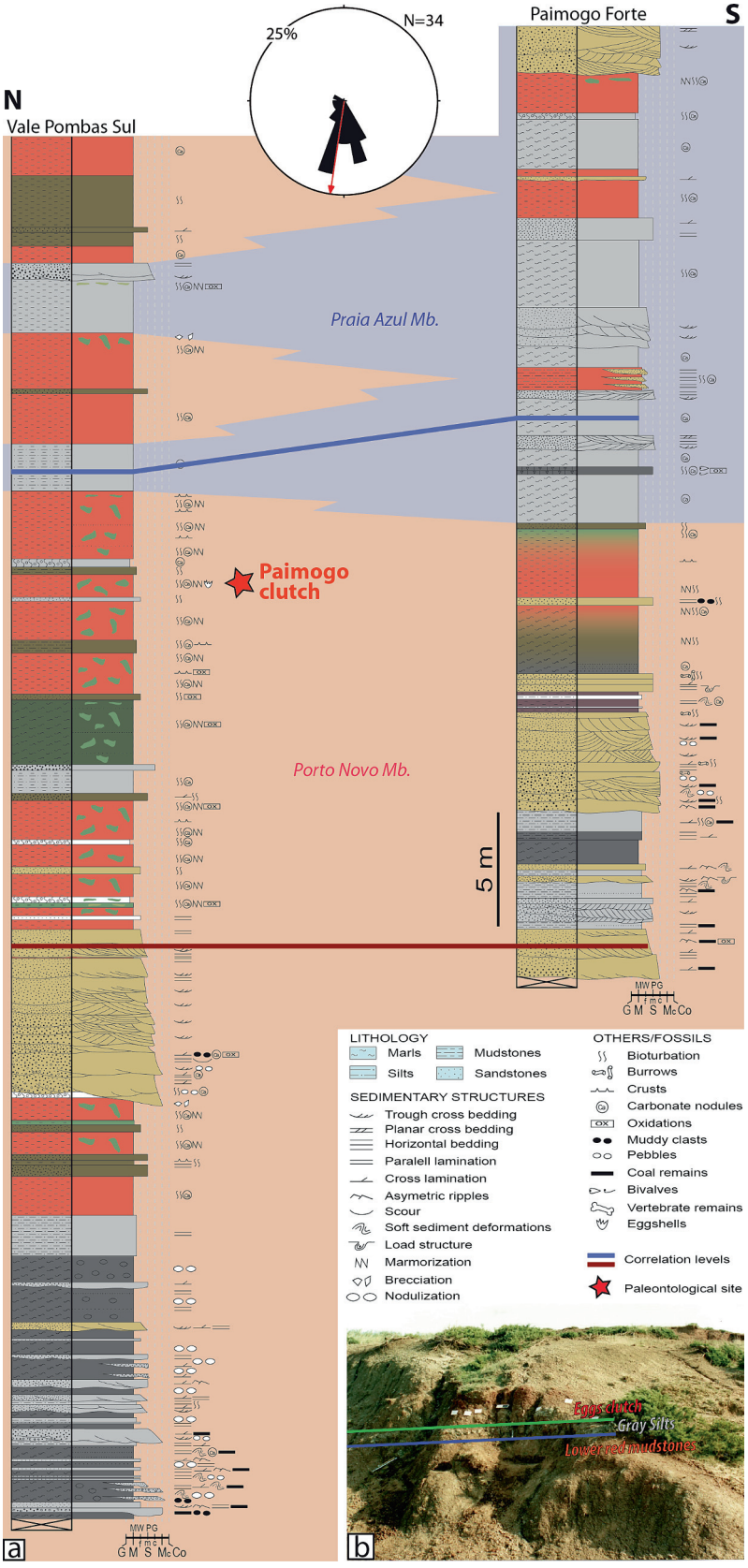

Fig. 2. (a) Main stratigraphic and sedimentology features close to the Paimogo site. (b) Detailed definition of this work units and egg-bearing layer in the original quarry (photo of the first diggings).

Table 1
Facies associations for the Porto Novo and Praia Azul mbs. in the Paimogo area.

Facies association	Lithology	Texture	Geometry and sedimentary structures	Interpretation
Sandstones	Sandstone (90%–100%)	Very coarse to fine-grained sandstone with rarely disperse pebbles and plant remains. Carbonaceous material is often preserved on lamination.	Channelled bodies and rarely tabular. Trough and planar cross-bedding. Parallel, cross- and ripple-lamination. Common fining-upwards cycles.	***Fluvial channels*** dominated by confined streams in less-cohesive banks and frequent lateral migration. During waning discharges some channels with longitudinal bars developed; Overbank areas poorly preserved.
	Conglomerate (0–10%)	Clast-supported textures and subangular to rounded pebbles. Fine sandy or silty matrix. Reworked carbonate nodules.	Decimetric erosive or irregular bodies with trough cross-bedding and cross-lamination.	
	Mudstone (0–10%)	Massive with occasional disperse pebbles.	Decimetric tabular or irregular bodies. Dessication cracks.	
Mudstones	Mudstone (70%–100%)	Massive. Yellow and green mottling. Spheric and elongated carbonate nodules.	Tabular bodies with occasional parallel-laminae. Rhizoliths, Root casts.	***Floodplains:*** mudflat areas fed by unconfined water flows and episodically reached by isolated shallow channels. Alternation between dry and near-surface water level favoured pedogenic processes. Locally permanent freshwater flooded areas also existed.
	Silt (0–20%)	Mainly massive.	Decimetric tabular bodies or with rare parallel and cross-lamination. Common root traces and burrowing. Carbonate nodules.	
	Sandstone (0–10%)	Coarse- to fine-grained sandstone with disperse pebbles. Massive or laminated.	Decimetric tabular or channelled bodies with trough cross-bedding, parallel or cross-lamination. Root traces and burrowing.	
Calcretes	Carbonate nodules (80%–100%)	Massive coalescent spheric and elongated carbonate nodules.	Decimetric tabular bodies. Structureless or ralrely prismatic structure.	***Floodplains*** with episodic clastic sedimentation rates and steady pedogenic processes.
	Mudstone (0–20%)	Massive or highly bioturbated.	Decimetric tabular bodies.	
Marls & Shelly beds	Marl (30%–80%)	Massive, bioturbated or brecciated with abundant vegetal remains.	Decimetric-metric tabular bodies with occasional parallel lamination. Common burrowing, root casts and carbonate nodules.	***Coastal plain – Interdistributary bays*** with mixing carbonate precipitation and detrital deposition. Marginal exposed areas with rooted vegetation. Frequent water-level oscillations. Shelly debris.
	Silts (0–20%)	Massive or laminated with common spherical carbonate nodules.	Decimetric-metric tabular or irregular bodies.	
	Shell (0–10%)	Massive.	Irregular bed with bivalves.	

4.1.2. Interpretation

The studied sections of the Vale Pombas Sul and Paimogo Forte are interpreted as having formed in a fluvial environment with low-sinuosity meandering streams and extensive adjacent floodplains, in areas located close to the shoreline. The observed features indicate that the fluvial influence was higher in the Vale Pombas Sul profile than in the Paimogo Forte profile, where marine and tidal processes imprinted their signal. The Paimogo egg accumulation appears in the floodplain deposits of the upper part of the Porto Novo Mb. close to the vertical and lateral change to the Praia Azul Mb. (Hill, 1988). If the deposits are referred to the stratigraphic division of Taylor et al. (2014), the succession corresponds to the São Bernardino and Porto das Barcas members, respectively.

The erosive bases, coupled with the sedimentary structures and fining-upwards trends, suggest that confined streams with common fluctuations in their discharge were predominant in the channels. Large bedforms were formed during high-energy events that transported significant amounts of bedload. The migration of the bedforms was high in the lower and middle parts of the channels, as suggested by the common cross-bedding, probably related to currents of $\sim$ 1 m/s (Allen, 1982). However, thin cross-laminations or ripples sandwiched between parallel-laminated sets suggest waning streams, reflecting low-current velocities during some stages (Allen, 1982; Collinson et al., 2006; Nichols, 2009). Despite the sedimentary structures, other criteria also suggest periodic fluctuations in the flow energy. Very coarse-grained sandstones with pebbles and muddy drapes at the bottom of highly incised channels correspond to lag deposits due to increasing energy conditions and reworking of the banks. Soft sediment deformations below and close to the thicker channels suggest a sharp overload as a consequence of high sedimentary rates (Owen, 1987; Hill, 1988; Moretti et al., 2001). By contrast, the interbedded mudstones with desiccation cracks and bioturbation reflect low-energy discharges and a deposition of high amounts of suspended material, probably during waning floods and subsequent subaerial exposure. Rarely, at the top of the channels, structureless mudstone and sandstone beds with a low angle of dip towards the banks could represent levees and crevasse splays (Allen, 1982; Hill, 1988). In addition, in the basal channel of the Paimogo Forte profile, tidal-induced characteristics in the sense of Martinius and Gowland (2011) are recognized. The intense burrowing in the topsets, coal debris and changes in the carbonaceous fragment concentration in the foresets of cross-laminae, and changes in the thickness, dip, and direction of the bottomsets can be interpreted as structures generated tidally during daily ebb-flood cyclicity.

The thick beds of fine-grained deposits correspond to overbank deposits in floodplains. The wide extent of these bodies, combined with localized crevassing, is interpreted as water-discharge that increased until the channel overflowed and gave rise to overbank sheet floods. The floods followed the regional slope towards the south like the channels. These areas were periodically exposed and pedogenized, as indicated by the mottling, rhizoliths, root casts, and scattered carbonate nodules. Rare calcretes and poorly developed horizons suggest a sedimentation rate sufficient to prevent soil horizontalization for much of the time (Hill, 1988). Grey burrowed and nodulized marls represent a mixed deposition of carbonate and terrigenous materials by suspension under the permanent water table. Additionally, the structureless, encrusted shelly bed reflects largely but not fully marine conditions, having probably been formed in interdistributary bay areas in delta plains (Hill, 1988) or low-lying coastal plains in the form of brackish-marine bays (Taylor et al., 2014).

4.2. Sedimentology of the Paimogo site

4.2.1. Description

The detailed study of the Paimogo site (Fig. 2b) focused on the sedimentological characterization of almost m-thick profiles between the blocks (seven profiles) and surrounding outcrops (four profiles) close to the place of excavation (Fig. 3a and Supplementary Data Fig. 2). The main lithological and sedimentological characteristics, especially the degree of pedogenesis, allow four units to be defined and a composite section to be formed (Fig. 3b).

Unit I (0.2 m-thick): red (2.5YR 4/8), massive silty mudstones present common green (5Y 7/4), subvertical, irregular mottling and elongated rhizohaloes (5 to 10 cm in length) with circular cross-sections (up to 1 cm in diameter) surrounding red millimetric rhizoliths (5R 4/6). The contacts between the mottling and the surrounding matrix are diffuse, whereas the elongated rhizohaloes and matrix show sharp contacts. The rhizoliths and rhizohaloes exhibit downward tapering, but some branching rhizoliths (5 cm-long and mm-diameter) are sporadically present. Irregular carbonate nodules up to 1 cm in diameter are scattered in the red matrix. Carbonate- or sand-filled root casts around 5 cm in length and 2 cm in diameter are present.

Unit II (0.1 to 0.2 m-thick): grey (5Y 7/1), micaceous silts to fine sandstones comprise a well-defined tabular bed towards the south and east, whereas in the blocks and westwards they are more irregular, interfingering with red silts (10R 3/6). In the lower part, relicts of cross-lamination are occasionally observed. Irregular carbonate nodules (<1 cm in diameter) are generally dispersed, but more spherical ones (up to 3 cm in diameter) appear concentrated close to the top. In the occasional interfingered reddish silt, green (5Y 7/4), subvertical, elongated rhizohaloes (4 to 7 cm in length) with elliptical sections show sharp contacts and downward tapering, becoming diffuse when they penetrate grey deposits.

Unit III (0.15 to 0.30 m-thick): red (10R 3/6) silts contain abundant spherical carbonate nodules (<2 cm in diameter) except for the upper part (~0.20 cm above the egg accumulation), where they are practically absent and a more light-coloured matrix (2.5YR 4/8) and yellow mottles (7YR 5/8) are present. Green rhizohaloes (7 to 10 cm in length) with elliptical sections and mottles (5 to 10 cm in diameter) form sharp and irregular diffuse contacts with the red matrix, respectively. The subvertical rhizoliths and rhizohaloes are less frequent at the bottom, becoming more abundant in the upper parts and towards the east. Furthermore, in the lower part rhizotubules are filled with carbonate, disappearing in the middle part (~0.10 cm below the egg accumulation), where eggshells become more abundant as far as the clutch. In this part and towards the top, small manganese nodules (<0.5 cm in diameter) are present.

Unit IV (>0.8 cm in thickness): red (10R 3/6), silty mudstones contain predominantly green (5Y 7/3), subvertical rhizohaloes (5 to 15 cm in length), showing circular cross-sections and sharp contacts with the surrounding matrix. Green rhizoliths (7 cm long and mm-diameter) with horizontal branching are less common and are limited to the uppermost zones, where yellow mottles (7YR 5/8) and mm-diameter manganese nodules also exist, and the matrix is light-coloured (2.5YR 4/8). The subspherical mottles of the lower zones are larger (up to 10 cm in diameter). Towards the southwest, iron-depleted zones are larger and more irregular with diffuse contacts between the haloes and the surrounding matrix. Carbonate nodules (<3 cm in diameter) and rhizotubules (~7 cm in length) are very frequent throughout the lower part of the unit.

The scarce palaeocurrent criteria found in Unit III (only 11 indicators, limited to isolated imbricated pebbles and poorly developed cross laminations) indicate a coherent S-trending flow in comparison with the overall area, the average being an SSW direction (Fig. 3a). In greater detail, different degrees of current-generated grain distribution are recognized in the thin sections, but all of them are consistent with the flow direction. The most common arrangement corresponds to dispersed subhorizontal grains mixed with aligned and imbricated grains (Fig. 4a). The long axes of elongated grains are parallel-oriented to the flow direction, and the flat faces of planar minerals show up-current and down-current imbrication (Fig. 4a,b). The current imprint could be high in some zones, resulting in a greater presence of oriented particles and occasionally in well-defined sedimentary structures such as cross-lamination (Fig. 4b,c). Thus, the settling and low-energy currents controlled the deposition and the sedimentary fabric, which could be locally disrupted by the secondary action of roots or nodulization, which reorganized the grains (Fig. 4d).

These primary and disrupted textural features show a good correlation with the grain-size curves and their spatial distribution. Grain-size analyses of samples from Unit III (blocks and outcrops) show clear differences in both statistical and graphical parameters between two subsets of samples (Fig. 5a). The first group presents a unimodal distribution close to 9.24 μm (mean value 20.07 μm, σ = 8.51) and symmetrical skewness, rarely with negative skew-

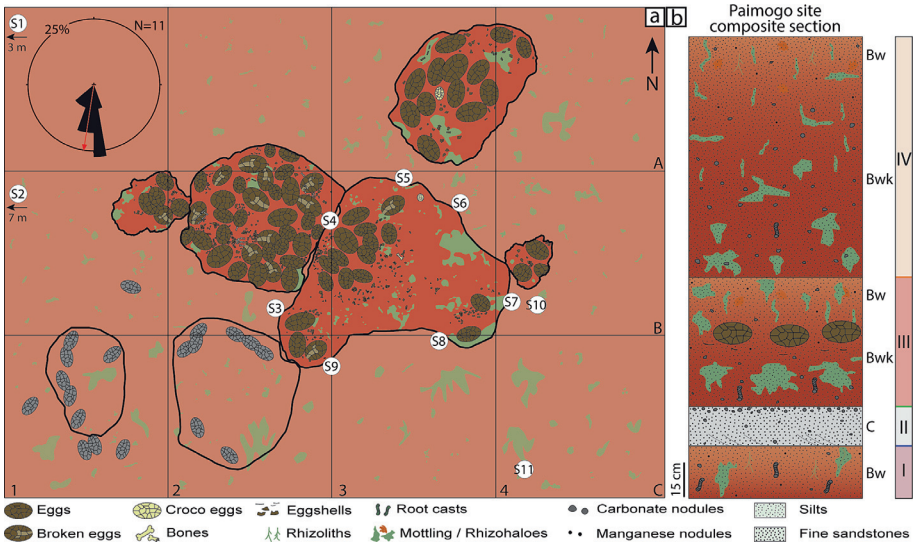

Fig. 3. (a) Mapping and reconstruction of the original Paimogo site with the location of the eggs and jackets. (b) Composite stratigraphic profile (cm-scale) of the Paimogo site.

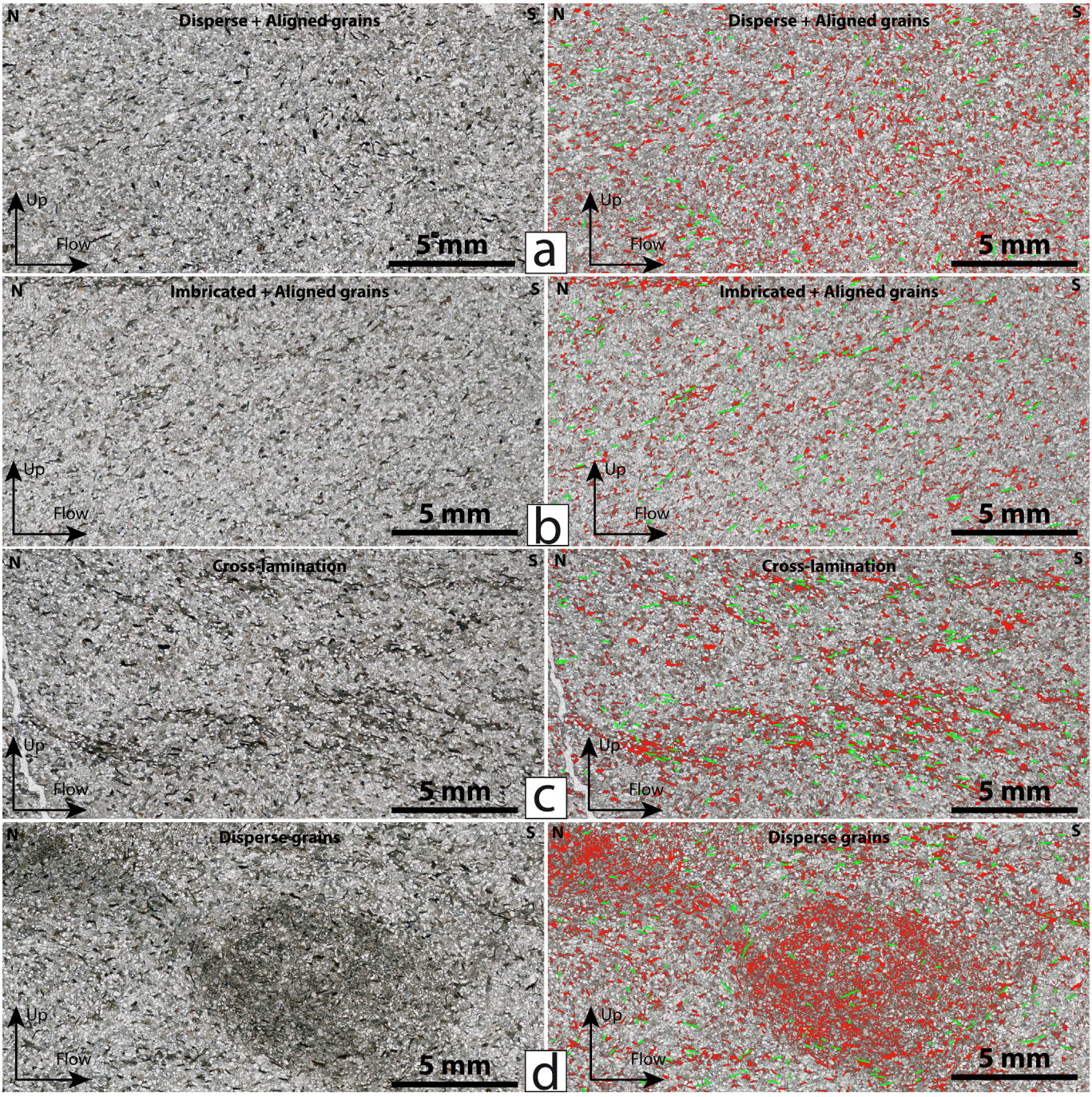

Fig. 4. Dispersion and alignment of the grains in the fabric of sediments from the Paimogo deposits. Left column shows the original optical microscope image, and in right column the elongated magnetic minerals appear coloured in green and red colors. (a) Mixed texture compounds of dispersed and aligned grains. (b) Aligned and imbricated grains. (c) Cross-lamination. (d) Disrupted texture by soft sediment remobilization.

ness, and with a mesokurtic curve (Fig. 5a). The second group shows greater variability, corresponding to grain-size bimodality and even trimodality and polymodality, of 8.97 μm, 123.41 μm, and 1050.52 μm (mean value 102.27 μm, σ = 81.49). The skewness is symmetrical or strongly positive, in curves with platykurtic, mesokurtic, and leptokurtic distributions (Fig. 5a). Moreover, all the samples of the first subset correspond to poorly sorted silts (medium grain-size), whereas the second subset varies from medium silt to very fine sandstones (very poorly sorted). These groups show a distinct arrangement around the eggs, the first group consisting of samples from the west of the midpoint of cell B3, whereas the second subset represents samples collected to the east of the same point (Fig. 3a). High-density bioturbation and pedogenesis can be recognized to the east, where the samples present multimodal curves associated both with changes in the flow velocity due to a vegetation barrier and disturbances induced by root penetration.

The organic matter content also shows the same pattern, there existing a slight variation in relation to cell B3 (Fig. 5b). The values of organic matter are significant throughout the palaeontological site. This contrasts with the absence of plant remains or coal (Fig. 3b). However, sediments to the west of cell B3 show around

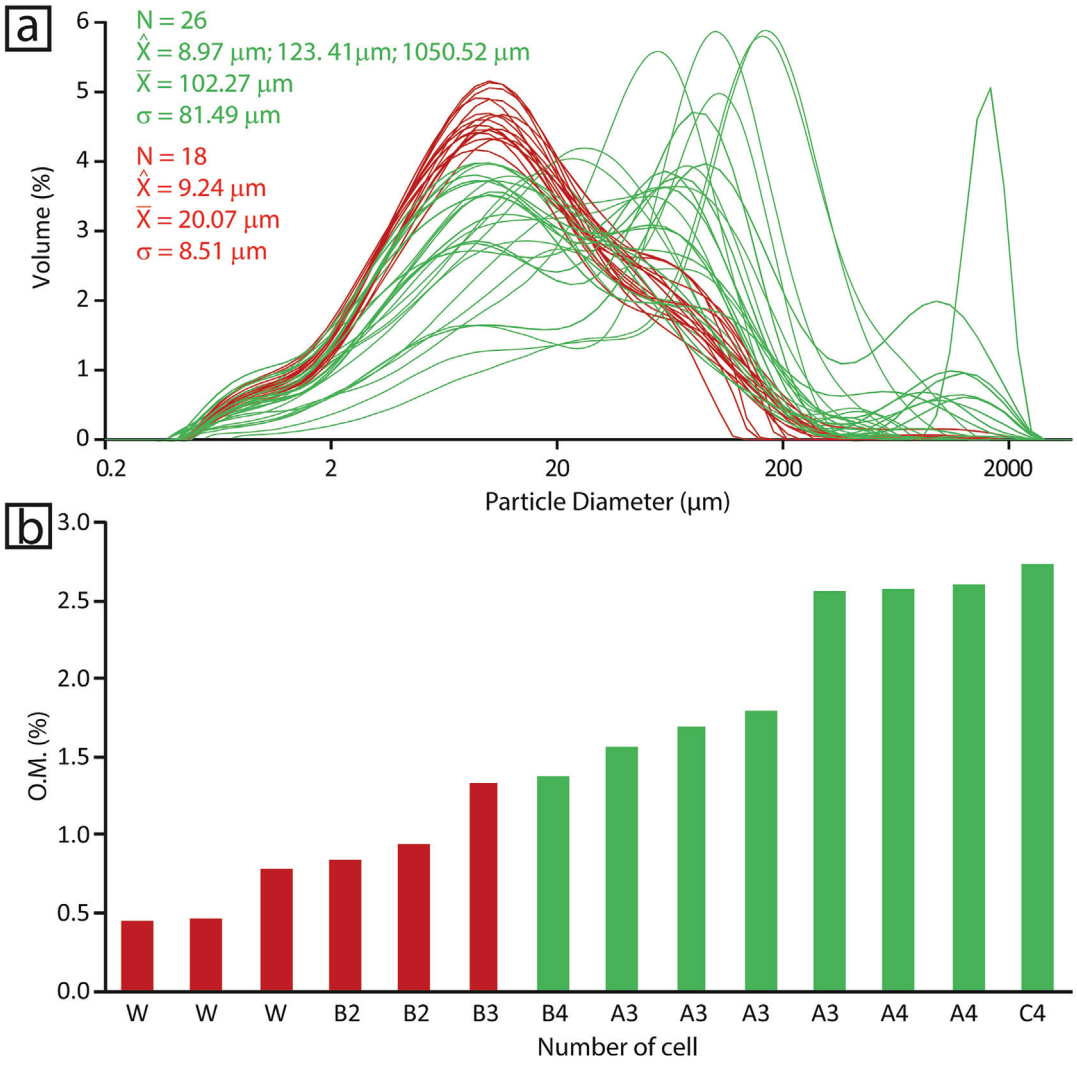

Fig. 5. (a) Grain-size distributions for Unit III samples coming from both, block and field. Size-frequency curves indicate two different flows recorded in the deposits, existing a mix of different particles in size as consequence of reworked processes. (b) Organic matter content of the Unit III sediments. The amount of OM increases towards the eastern samples and in the field samples when they are compared to blocks ones.

1.5% less organic matter than those to the east. The slight increase in organic matter to the east also shows a good correlation with the increases in pedogenesis and root traces (Fig. 3a).

4.2.2. Interpretation

The parent material of the palaeontological site is composed of poorly sorted silts that preserve the primary sedimentary fabric at mm-scale. Grain size, sorting, and composition between matrix and rhizohaloes are similar, and only minor disturbances and realigned grains due to root penetration are observed, indicating low pedogenic modification (Retallack, 1988; Mack et al., 1993). The palaeosol profile corresponds to alternating Bw-Bwk horizons and local Bw-Bwk-C horizons, without clear evidence of A horizons such as light colours, enrichment in organic matter, or high-density rhizoliths (Fig. 3b). The Bw horizons are characterized by frequent green mottles, and subvertical rhizoliths and rhizohaloes are more abundant, suggesting a key contribution of the roots in iron mobilization (*e.g.*, Kraus and Hasiotis, 2006). Yellow mottling reflects a preferential mobilization of hematite against goethite under subanoxic conditions during short-seasonal wet periods (Kraus and Hasiotis, 2006). The near-absence of clays or coatings suggests a low degree of clay formation and illuviation during the soil development process (Buol et al., 2011). Moreover, pedogenic manganese nodules indicate fluctuating moisture conditions (Retallack, 1988), and the low content in carbonate nodules suggests a certain degree of leaching to the Bwk horizon. The transition between Bw and Bwk is marked by a progressive enrichment in carbonate nodules without a well-developed boundary. In the Bwk horizons, the nodules remain isolated in a poorly cemented matrix (early stage II of Machette, 1985), and carbonate-filled root casts combined with irregular, iron-depleted masses suggest fluctuations in the moisture (*e.g.*, Kraus and Hasiotis, 2006). The C horizons correspond to fine sandstones that preserve the original lamination, but a high density of carbonate nodules close to the upper boundary indicates an incipient development of a Ck horizon in relation to the lower part of a Bwk horizon in some zones.

The coexistence of primary sedimentary structures and a low degree of pedogenesis represents a palaeosol profile predominantly characterized by very weakly developed horizons and moderately well-drained conditions (Retallack, 1988; Mack et al., 1993; Kraus, 1999; Kraus and Hasiotis, 2006; Catena et al., 2017). The irregular boundaries of the palaeosol profiles, thin horizons with gradual limits, and preserved sedimentary structures point to a classification as Entisol (Soil Survey Staff, 2010; Buol et al., 2011). The very poor development of ferric and calcic horizons as well

as the prominent pedogenic character can be attributed to a calcic Protosol (Mack et al., 1993), the Bwk horizons belonging to the early stage II of Machette (1985).

The lack of a recognizable A horizon suggests a slightly truncated palaeosol due to sediment removal (*e.g.,* Morrison, 1964; Kraus, 1999). The alternation of very weak Bw and Bwk horizons reflects a stacked compound profile, which is characteristic of zones near to avulsion belts, probably located < 2 km from the main channel (Marriott and Wright, 1993; Kraus, 1999). In these zones, unsteady sedimentation occurred in rapid flooding events with short recurrence periods rather than soil development, resulting in the burial of the immature older soil horizon and a partial overlap with the younger palaeosol (*e.g.,* Kraus and Alsan, 1993; Catena et al., 2017; Lucas and Tanner, 2021). To the south and southeast of the Paimogo area, the palaeosols are composed of finer sediments, and cumulative profiles have been established, showing more distal areas in the floodplain. Although red matrix and carbonate accumulations indicate moderately well-drained conditions, the mottling is associated with short periods of wet conditions, probably after flooding or high-precipitation events in which the water table was raised (Kraus and Hasiotis, 2006). In addition, the root traces display changes in the redox conditions due to fluctuations in the water saturation (Kraus and Hasiotis, 2006; Catena et al., 2017). Thus, semiarid conditions prevailed, but the water supply was enough to maintain vegetation cover, perhaps due to the intensive seasonal rains that also provoked the channel overflows. In light of the above, the time taken to form the soils could range on the order of between 10^1–10^2 years, but the scarce carbonate content points to a greater formation time of around 10^2–10^3 years (Machette, 1985; Birkeland, 1999; Daniels, 2003).

5. The Paimogo egg accumulation

5.1. Egg distribution and geometry of the accumulation

The Paimogo egg accumulation contains at least 73 complete to partially complete eggs, indeed up to 100 according to the filed reports that count the eggs contained in the unopened and lost jackets. These are attributable to theropod dinosaurs and are clustered in four to six groups of variable size (Fig. 3a). Three isolated crocodile eggs were found in the external areas of the groups, but these follow the same arrangement (location and orientation in the clutches) as the dinosaur eggs. The main cluster is located between cells B1 to B3, comprising 52 eggs in close proximity to each other in a subelliptical grouping (NW-SE oriented). In the centre of the assemblage, the long axes of the eggs are more randomly oriented, whereas towards the boundaries NW-SE and NE-SW orientations are present (Fig. 3a). The second cluster (cells A3 – A4) is formed by 13 eggs closely associated in an asymmetric NE-SW-trending ellipsoid in which the outer eggs also present preferred NW-SE and NE-SW orientations of the long axes. Two smaller clusters are formed by at least three eggs that are very close together (cells B2 – C2), of which there may be more if the unopened jackets is taken into account, and five scattered eggs between cells B3 and B4. Around the assemblages, a high number of eggshells appear both concave-up and concave-down, but it is noticeable that they decrease in abundance further east from the main group throughout cell B3.

As regards the vertical distribution, the eggs are in two to three superposed levels without significant amount of sediment between them. A general imbrication pattern can be observed in the egg-to-egg contacts, with the westward eggs resting on the eastward ones. The two long axes of the eggs are always in a subhorizontal position, whereas the short axes are close to the vertical. Within the stratum, the eggs always occur in the middle part of Unit III within the Bw horizon, and they are filled with the same surrounding red silty material. Some of them, especially in the minor clusters, contain green fills associated with circular breakages of the top parts of the egg (<3 cm in diameter). These broken eggs show vertical eggshell fragments collapsed down into the egg. Green tones have also frequently been recognized in the underlying materials of the crushed eggs. Three eggs with putative hatching windows can be identified in the main group, coinciding with an abundance of ex ovo perinatal bones.

5.2. Egg and eggshell features

5.2.1. Description

The eggs of the Paimogo accumulation are crushed due to lithostatic pressure and diagenetic processes, but their original shape can be estimated. They are centimetric in size (100 mm × 70 mm) and have a prolate shape, with an average ellipsoid ratio of 1:6. By comparison with previous studies of the accumulation, our inferred size for the egg is slightly smaller and more elongated (contra Mateus et al., 1997; Antunes et al., 1998). This is due to the larger number of eggs sampled and measured for the present study.

The mean eggshell thickness is 769 μm (N = 54, SD = 0.94). This value is significantly lower than the previously reported mean thickness of 700 to 1000 μm (Mateus et al., 1997) or 920 ± 110 μm (Antunes et al., 1998) due to the presence of a secondary diagenetic layer of calcite covering the outer surface of most of the eggs. Previous reports described this secondary layer as being the result of the recrystallization of the outer part of the eggshell, but detailed observations using thin sections and SEM suggest that it is indeed an epitaxial overgrowth of secondary calcite on top of the eggshells (Fig. 6). The large standard deviation observed in the sample is attributed to differences in the degree of reabsorption of the mammillae. In general, the eggs have a smooth outer surface, and no abrasion or erosion marks are observed (Fig. 6a). On the inner surfaces, the mammillae are well preserved in most of the eggs, with varying degrees of mammillary reabsorption (Fig. 6b).

The eggshells show a two-layered obliquiprismatic morphotype, with a mammillary layer to continuous layer thickness ratio of 1:3 to 1:4 in well-preserved eggshells. The mammillary layer (ML) and a continuous layer (CL) with horizontal growth lines occasionally show a recrystallized prismatic layer or secondary calcite deposits. The shell units are relatively wide (390 μm, N = 51, SD = 75; shell unit height/width ratio of 2.5:1) and show a sharp columnar extinction pattern in cross-polarized light (Fig. 6 and Supplementary Data Fig. 3). The ML shows a radial calcite ultrastructure, with thin wedges of calcite radiating from the preserved organic cores. The transition between the ML and the CL is gradual (Fig. 6a), although some eggshells show an apparently more abrupt transition due to diagenetic alteration (Fig. 6b). The CL shows a tabular ultrastructure, without any vesicles or squamatic ultrastructure, where prisms can be distinguished in SEM images. The eggshell has wide, relatively scarce, oblique pore channels (0.180 μm in diameter, Fig. 6c), and a pore density of 0.16 pores/cm^2 (Antunes et al., 1998). The pore system is obliquicaniculate to angusticaniculate. The pores are almost straight, circular in section, and constant in diameter throughout their length, the angle to the shell surface ranging from 60° to 90° (Antunes et al., 1998). Most pores are filled with secondary calcite deposits, which are similar in composition, texture, and grain size to the secondary diagenetic layer that covers the external surfaces (Fig. 6e), confirming the diagenetic origin and epitaxial formation of the latter. Pore openings are difficult to observe on the external surfaces. The inner surface shows the preserved mammillary bases (Fig. 6e).

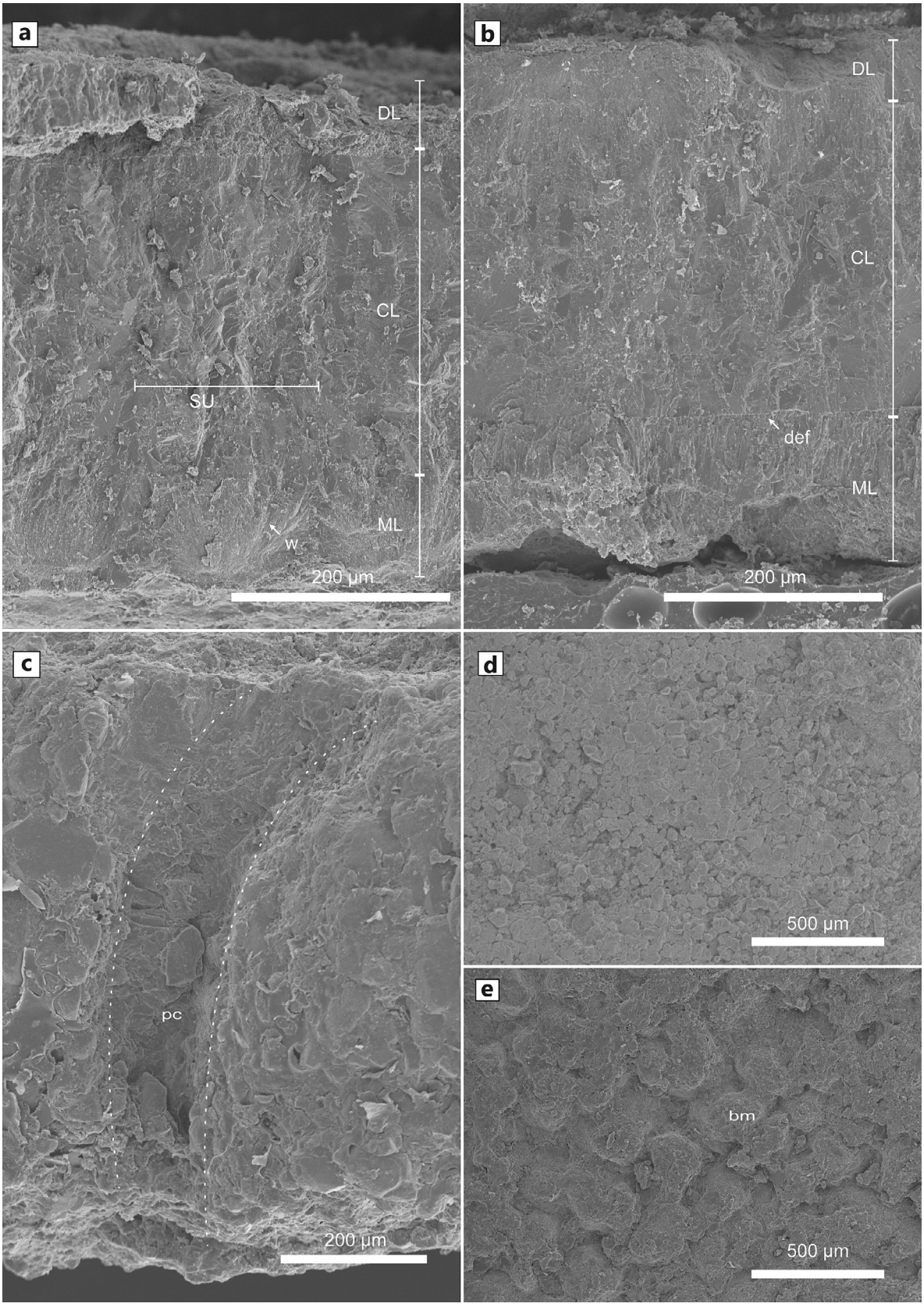

Fig. 6. Secondary electron images of Preprismatoolitus sp. ML 565. (a) ML 565-Egg 29. Radial section of the eggshell, showing relative wide Shell units with a mammillary layer composed of radiating wedges of calcite and a gradational transition to a continuous layer with tabular ultrastructure. Shell units can be distinguished through the complete eggshell thickness. (b) ML 565 Egg 5. Radial thin section of the eggshell showing an apparent abrupt transition between the mammillary layer and the continuous layer due to *a*-crystallographic defect. (c) ML 656-Egg 8. Radial thin section showing an oblique pore channel. (d) ML 656-Egg 8. Outer surface view of the eggshell showing the irregularly crystallized outer diagenetic surface covering the smooth outer surface. (e) ML 656-Egg 8. Showing mammillary bases with no reabsorption craters. Abbreviations: ML, mammillary layer; CL, continuous layer; DL, diagenetic layer; SU, shell unit; def, crystalline defect; pc, pore channel; bm, base of mammilla.

5.2.2. Interpretation

The obliquiprismatic morphotype as well as the eggshell thickness and egg size are compatible with the oogenus *Preprismatoolithus* (Hirsch, 1994), first described in the contemporary Morrison Formation (USA). The specimens are thinner than the only described oospecies, *Preprismatoolithius coloradensis*, which has a slightly greater range of eggshell thickness, from 700 μm to 1000 μm. This eggshell has been associated with allosauroid theropod dinosaurs on the basis of fragmentary embryos showing diagnostic characters of the genus *Allosaurus* (Carrano et al., 2013).

The association of the Paimogo eggs with a theropod taxon was unambiguously established in the original description of the accumulation (Mateus et al., 1997, 1998) on the basis of the morphology of the femora and tibiae. More precise details of this classification have been suggested, with several works attributing the eggs and embryos of Paimogo to the allosauroid theropod *Lourinhanosaurus antunesi*, on the basis of the similar age and geological proximity, the relative proportions of the centra of the presacral vertebrae (Ricqlès et al., 2001), and the presence of a large premaxilla showing four alveoli, which is unlike *Allosaurus* (Carrano et al., 2013). However, both studies predate the description of two new allosauroid theropod species from the Lourinhã Formation: *Allosaurus europaeus* and *Lusovenator santosi* (Mateus et al., 2006; Malafaia et al., 2020). Further detailed taxonomic studies of the embryonic material are needed to improve the taxonomic attribution of the Paimogo egg assemblage.

Antunes et al. (1998) studied the porosity of the eggs from the Paimogo assemblage, obtaining a water vapour conductance of 483 mg $H_2O{\cdot}day^{-1}{\cdot}Torr^{-1}$, concluding that aerial incubation would have caused the death of the embryos due to excessive water loss as a result of the diffusion of water vapour (Deeming, 2006, and references therein). Our calculated water vapour conductance of 179 mg $H_2O{\cdot}day^{-1}{\cdot}Torr^{-1}$ is significantly lower on account of the newly obtained values for egg size and eggshell thickness, despite measuring a similar pore density (0.194 versus 0.19 pores/mm^2) and pore diameter (0.16 mm of max diameter versus 0.18 mm of max diameter) as Antunes et al. (1998) reported, but it is still times the expected water vapor conductance for an avian egg of similar weight (Table 3 and Supplementary Data Fig. 4). This value of water vapor conductance is similar to those of modern, mound-nesting crocodiles such as *Crocodylus porosus* (375 mg $H_2O{\cdot}day^{-1}{\cdot}Torr^{-1}$) and *Alligator mississippiensis* (387 mg $H_2O{\cdot}day^{-1}{\cdot}Torr^{-1}$) (Deeming, 2006). Water vapor conductance alone does not provide enough information to differentiate dug *vs.* mound nesting clutches, but strongly suggests the eggs of Paimogo were laid and covered to avoid desiccation.

5.3. Geochemistry of the eggshell

5.3.1. Description

The geochemical analyses of the eggshells establish two subsets of eggs based on $\delta^{16}O$, $\delta^{13}C$, and Sr/Ca values (Supplementary Data Table 1). Group A (33 eggs) corresponds to lower values in the oxygen and carbon isotopes and higher Sr/Ca ratios, whereas Group B (18 eggs) is characterized by higher isotopic values and lower Sr/Ca ratios (Fig. 7a). The altered eggshells tend to be similar to the signature of the carbonate nodules and carbonate root casts (Supplementary Data Table 1) (Coimbra et al., 2023). There is a correlation between the two geochemical types, and the egg-size proportions reflect a clear correspondence, pointing to individual and parallel tendencies for each group. Both groups fit well with the average elongation coefficient, and the ranges of length are similar, but Group A consists of larger eggs than Group B (Fig. 7b). The 19 altered eggs present the same proportions as Group A, whereas the non-analysed eggs show an intermediate distribution between the sizes of the two groups.

In addition, the distribution of the egg groups in the accumulation also varies in terms of longitudinal axis orientation and spatial arrangement (Fig. 8). Within the overall orientations, NW-SE and N-S trends stand out against a background where other secondary maxima such as NE-SW and ESE-WSW can be recognized. Group A shows almost the same pattern with maxima in N-S (clockwise deviation) and NW-SE, whereas Group B presents a clear maximum close to N-St (anticlockwise deviation) and a significant secondary maximum in NNE-SSW (Fig. 8). The orientation of the altered eggs is perfectly consistent with the Group A pattern, corresponding to the main and secondary trends of this group. The unanalysed eggs are closer to the Group A distribution, at least the conspicuously NW-SE trending eggs, and the two secondary NE-SW and ESE-WSW orientations are represented in both groups. Furthermore, the spatial arrangement of Group A is predominantly in the centre of the accumulations, and the eggs in Group B form a crescent shape surrounding the Group A eggs (Fig. 8).

5.3.2. Interpretation

The best-known theropod nests and clutches point to the construction of individual mounds or to egg-laying on the ground surface, using various methods of cover such as sediment, vegetation, or active incubation in order to prevent dehydration (*e.g.*, Carpenter, 1999; Zelenitsky, 2006). The term mound has been used as a morphological description instead of the genetic origin, describing a non-cohesive positive relief above the ground. Each individual structure contains between 14 and 28 eggs and is attributed to a single female laying. The occurrence of several mounds close together has been interpreted as colonial behaviour with several females in a common nesting area (*e.g.*, Carpenter, 1999). Regardless of whether it is a collective laying or remodelled mounds, the number of eggs in the Paimogo accumulation would have required several females or one female in several periods (Supplementary Data Fig. 5). The geochemical values and the average size of the dinosaur eggshells point to the presence of at least two females, independently of the control factor over the isotope signal. Traditionally, biogenic carbonates such as dinosaur eggshells are commonly interpreted as deposited at near oxygen isotope equilibrium with the ambient temperature (*e.g.*, Erben et al., 1979; Sarkar et al., 1991; Cheong-bin et al., 2009; Domingo et al., 2013). Recently, small shifts in the clumped isotope signature have been interpreted as vital effects during eggshell precipitation due to variations in body temperature and mass, even within the same species (Dawson et al., 2020; Laskar et al., 2020). The higher isotope values of Group A in comparison with the lower values of Group B would imply the same two hypotheses expounded above to explain the accumulation. However, the Sr/Ca ratio is controlled only by environmental conditions, no metabolic influence being known in continental vertebrates, with low values referring to arid periods and high values to wetter periods (Cojan et al., 2003; Grellet-Tinner et al., 2012). In the Paimogo eggshells, the $\delta^{16}O$, $\delta^{13}C$, and Sr/Ca values indicate a correspondence that suggests an influence exerted by the environmental conditions and the drinking water, Group A being associated with streams and fresher waters and Group B with more stagnant, evaporating waters.

Even though the eggs are intact and apparently preserved *in situ*, the geometrical arrangement is compatible with water transport since they were located in the same horizon and in close proximity. No evidence of transport is recognized, such as rounding or abrasion in individual eggshells, or smashed and battered eggs, suggesting a parautochthonous assemblage resulting from short-distance transport (*e.g.,* Cheong-Bin et al., 2009; Oser and Jackson, 2014). The orientations of the longitudinal axes parallel and perpendicular to the inferred palaeocurrents reflect imbrication and transport by rolling, the behaviour shown by any sedimentary particle in a water flow. The amount and arrangement

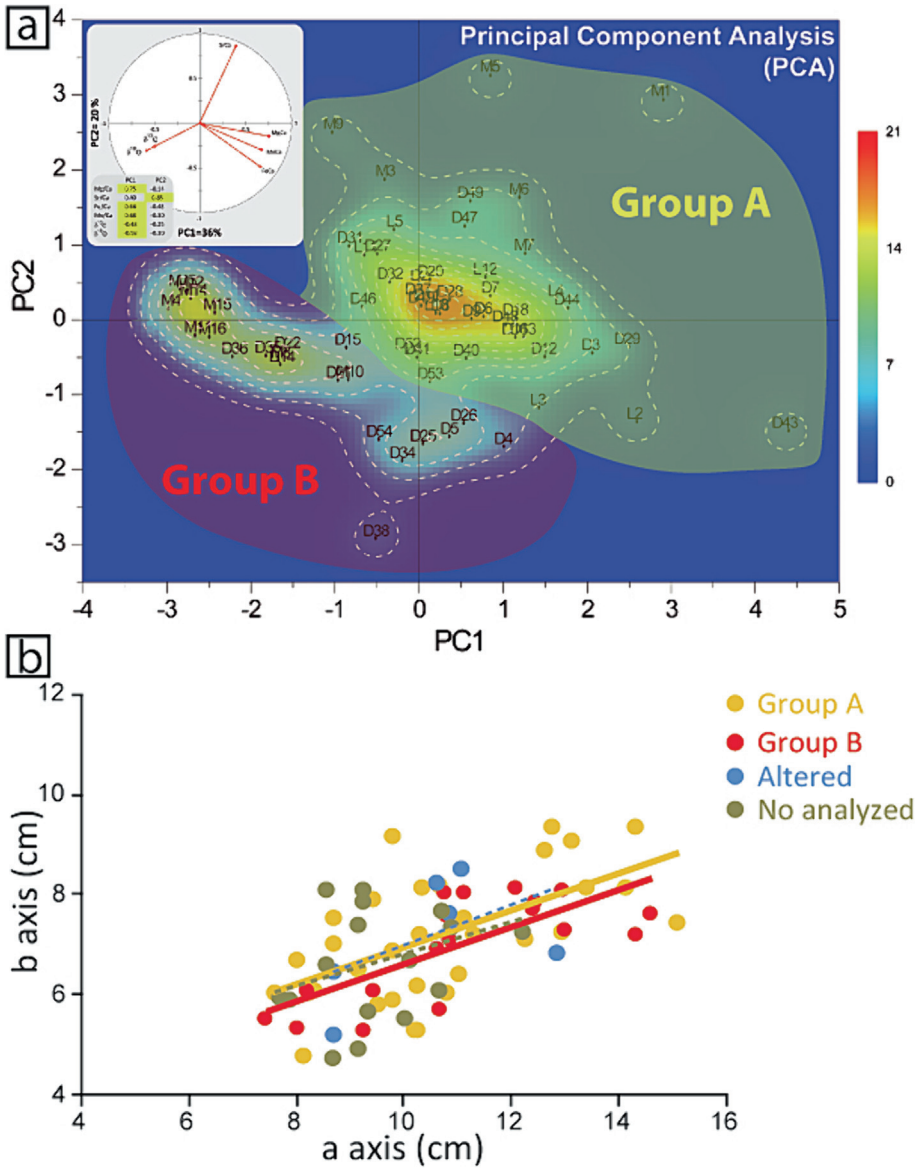

Fig. 7. Geochemical results for all eggshells analysed in this work. (a) Principal Component Analysis of the data based on Mg/Ca, Fe/Ca, Sr/Ca, Mn/Ca, $\delta^{16}O$ and $\delta^{13}C$ indicates two possible groups of different eggs. (b) Graphical relation between the length of the axes for the several egg groups, indicating a different proportion between them.

of the eggs belonging to Group A suggest less transport than the eggs in Group B. A remodelling of several mounds belonging to a collective assemblage thus seems most probable.

Only three eggs show a clear dissolution of the mammillae as a consequence of the embryo's calcium requirements, and four eggs are opened by hatching or cracking. Due to the paraautochtonous nature of the assemblage, it is unlikely the eggs hatched. Across the accumulation, four assemblages of embryo bones are recognized, three of them associated with Group A eggs and only one with Group B. These criteria are coherent with a low rate of success in the clutches. If clutches where viable at the moment of the flood, movement of the eggs may have induced and important stress on the embryos and an early interruption of the incubation.

The clutches probably consisted of mounds covered by sediment or vegetation (and abandoned as a consequence of the water rising) since they were easily destroyed and remodelled. The moderately well-drained conditions and the redox processes, typical of such semiarid environments, prevented the preservation of the plants and organic matter. However, the considerable amount of organic matter preserved around the eggs suggests that vegetation cover could have been used to protect the eggs and maintain the warm, moist conditions. It seems improbable that the eggs were laid on the ground surface since the egg conductance would have resulted in the dehydration of the embryos (Antunes et al., 1998; Carpenter, 1999).

6. AMS analysis of the Paimogo egg-bearing sediments

6.1. Anisotropy of magnetic susceptibility

A summary of AMS properties for the samples as a whole and for each subsite (per bed and location in block or outcrop) is shown in Table 2. The analysis was based on 158 reliable specimens, whereas 32 specimens were excluded from the subsequent analyses after filtering the data, since they presented vertically oriented grains corresponding to mechanical inverse fabric (compared to the assumed horizontal sedimentary plane, Bradák et al., 2020)

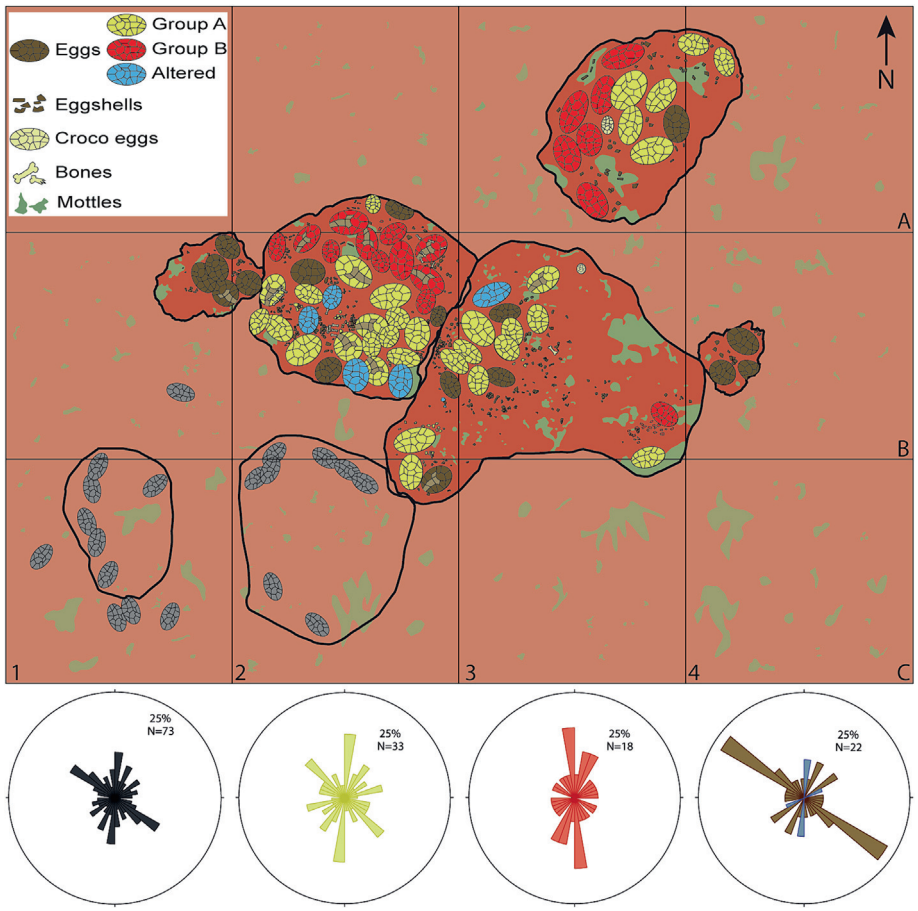

Fig. 8. Mapping of the egg distribution and orientation along of the Paimogo site, considering the different groups. In the lower part, rose diagrams show the graphical distribution of the mayor axis in each case.

Table 2
Magnetic susceptibility data of the Paimogo site.

Site	Specimen group	*N*	Km ($\times 10^{-6}$)	SD ($\times 10^{-5}$)	*Pj*	*T*	*L*	*F*	*q*	K_{max} (T/P)	Conf Ang (°)	K_{int} (T/P)	Conf Ang (°)	K_{min} (T/P)	Conf Ang (°)
Total	**Complete**	**158**	**158**	**3.51**	**1.015**	**0.545**	**1.003**	**1.011**	**0.279**	**351/8**	**62/13**	**081/3**	**62/11**	**220/86**	**13/11**
	Blocks	95	162	3.27	1.013	0.463	1.003	1.009	0.335	352/6	19/3	082/5	19/3	212/82	13/12
	Outcrops	63	154	3.82	1.018	0.668	1.003	1.014	0.194	182/0	85/10	092/1	90/5	290/88	3/3
Unit III (Egg laid bed)	**Complete**	**82**	**158**	**3.49**	**1.015**	**0.557**	**1.003**	**1.011**	**0.272**	**344/2**	**59/11**	**074/3**	**59/13**	**228/86**	**13/11**
	Blocks	50	155	3..49	1.013	0.461	1.003	1.009	0.339	343/1	53/13	079/6	53/13	240/83	14/13
	Outcrops	32	163	3.60	1.018	0.707	1.002	1.014	0.167	351/2	74/10	081/0	74/12	178/88	6/4
Unit II (Mid. grey bed)	**Complete**	**45**	**151**	**15.1**	**1.013**	**0.513**	**1.003**	**1.009**	**0.295**	**002/4**	**47/12**	**092/2**	**47/10**	**207/85**	**13/10**
	Blocks	24	160	16.0	1.012	0.413	1.003	1.008	0.357	008/9	32/11	098/2	32/12	198/79	12/11
	Outcrops	21	141	14.1	1.014	0.626	1.002	1.011	0.224	157/2	70/8	066/0	70/9	327/88	9/8
Unit I (Low. red bed)	**Complete**	**31**	**168**	**2.98**	**1.019**	**0.559**	**1.003**	**1.014**	**0.264**	**015/3**	**75/15**	**107/1**	**75/10**	**224/87**	**16/9**
	Blocks	22	173	2.53	1.016	0.540	1.003	1.012	0.278	005/10	48/12	275/11	48/8	181/80	13/8
	Outcrops	9	156	3.77	1.026	0.606	1.005	1.020	0.231	077/4	60/8	166/7	60/10	315/12	10/7

caused by geological/pedological processes and generally corresponded to high K_m values and prolate subvertical ellipsoids (Fig. 9). Most of them, both from the blocks and outcrops, were located towards the east and displayed bioturbation structures, which were likely the result of the mechanical and chemical activity of roots.

The overall calculated mean susceptibility (K_m) is 158.5×10^{-6}SI units, ranging from 74.3×10^{-6} to 2237×10^{-6}SI units, with an almost normal distribution and most of the values (~90%) between 106.4×10^{-6} and 219.4×10^{-6}SI units (Fig. 9a). This suggests the important contribution of paramagnetic particles to the bulk susceptibility, corroborated by the hyperbolic progressive decay of the initial part of the thermomagnetic curves (see Appendix: Supplementary Data Text and Supplementary Data Fig. 6). The mean value of the corrected degree of anisotropy (*Pj*) is 1.015, ranging between 1.012 (Unit II block) and 1.026 (Unit I outcrop), whereas the egg bed (Unit III) displays values very close to the average and between the subsites, 1.013 and 1.018 in blocks and outcrops, respectively (Table 2). Most of the specimens show an oblate shape parameter (T), and most of the values, around 90%, are between 0.230 and 0.970, except for 16 specimens that show prolate or triaxial ellipsoids ranging from − 0.521 to 0.168

Table 3
Selected measures of eggshell physical properties and calculated values.

Measure	Variables and formulas	N	Value	Units	Reference
Egg length	L	73	100	cm^2	This work
Egg width	B	73	70	cm^2	This work
Pore type	–	–	oblique	–	Mateus et al., 1997; this work
Egg mass	$M = 5.60{-}4E^{*}LB^{2}$	–	2479.4	g	Deeming and Ferguson, 1991
Surface area	$A_s = 4.835\ M^{0.662}$	–	209	cm^2	Paganelli et al., 1974
Surface area (ellipsoid)	$A_{se} = 4{\cdot}\pi{\cdot}[1/3^{*}((a{\cdot}b)^{1.6075}+(a{\cdot}c)^{1.6075}+(b{\cdot}c)^{1.60753})]^{1/1.6075}$	–	199	cm^2	This work
Egg volume (ellipsoid)	$V = 4/3^{*}\pi^{*}(L/2)^{*}(B/2)^{2}$	–	2.57E + 05	mm^3	This work
Number of eggs (measured)	N_{Em}	–	73	eggs	This work
Number of eggs (estimated)	N_{Ee}	–	100	eggs	Mateus et al., 1997
Clutch volume (minimal)	V^{*}NEm	–	1.87E + 07	mm^3	This work
Mean eggshell thickness	L_s	56	0.769	mm	This work
Pore density	P_d		0.194	$Pores^{*}mm^{-2}$	This work
Number of pores (estimated)	N	–	3860.6	Pore openings	This work
Pore opening radious (max)	$r+$	111	0.076	mm	This work
Pore opening radious (min)	$r-$	111	0.065	mm	This work
Pore opening area	A	111	0.017	mm^2	This work
Total pore opening area	$A_p = A^{*}N$		65.6302	mm^2	This work
Calculated water vapour conductance	$G_{H_2O} = A_p(0.477L_s)^{-1}$		178.92	$mgH_2O^{*}day^{-1}{*}Torr^{-1}$	Ar and Rahn, 1985
Mass specific water vapour conductance	SpG_{H_2O}		0.07	$mgH_2O^{*}day^{-1}{*}Torr^{-1}{*}g^{-1}$	Ar and Rahn, 1985
Predicted water vapour conductance			39	$mgH_2O^{*}day^{-1}{*}Torr^{-1}{*}g^{-1}$	Deeming, 2006

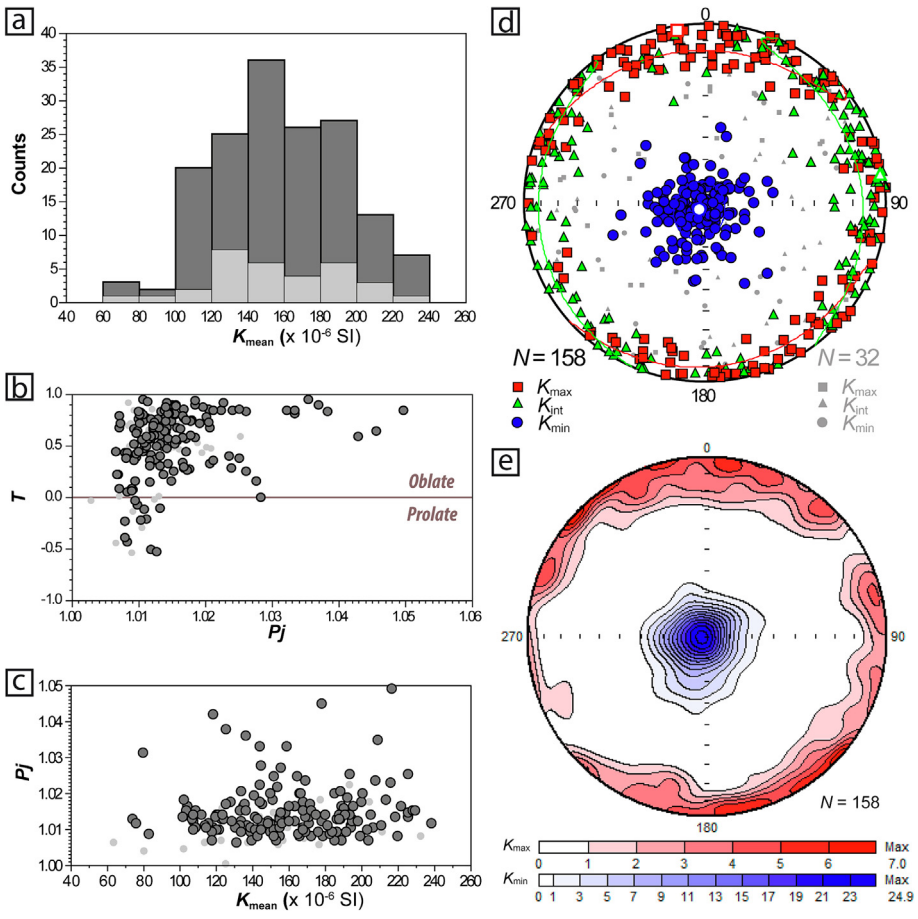

Fig. 9. Graphical plots of the mean magnetic fabric of the all studied specimens. (a) Frequency for the total range of mean susceptibility values (km) in the study and discarded samples. (b) Jelinek diagram. (c) Magnetic susceptibility (km) *vs* corrected anisotropy degree (*Pj*). (d) Equal area projection of the three magnetic axes after restoring bedding to horizontal, including their confidence ellipses. K_{max} in red squares, K_{int} in green triangles and K_{min} in blue circles. The larger symbols indicate the average value for each axis. (e) Contour diagrams with the statistical distribution of magnetic lineations. The red and blue coloured areas represent the directions of K_{max} and K_{min} axis, respectively.

(Fig. 9b). The mean value of the magnetic lineation (L) is 1.003, and this always displays low variation (<0.002) when the subsites for the same bed are compared (Table 2). The values of magnetic foliation (F) are fairly similar to the overall mean value of 1.011, varying between 1.008 (Unit II block) and 1.020 (Unit I outcrop), the values of 1.009 and 1.014 of the egg bed subsites (Unit III) being very consistent with each other and again with the average (Table 2).

All the magnetic fabrics were rotated into tilt-corrected coordinates, and the overall mean AMS ellipsoid (Fig. 9d,e; Supplementary Data Fig. 7) displays a K_{min} clustering close to the centre of the projection and perpendicular with respect to the bedding plane, where K_{max} and K_{int} form a nearly horizontal girdle (95% samples < 30°). The clusters of the K_{min} axes in the different subsites show confidence angles close to the mean value for the overall zone (13°/11°), indicating a better grouping in the outcrop subsites than in the block ones (Table 2, Supplementary Data Fig. 7). This can be explained by higher errors (or accumulated errors) in the orientation of the samples extracted from blocks, compared to those directly extracted in the outcrop. Although K_{max} and K_{int} are scattered in the bedding plane, a preferred trend to N-S orientation for the magnetic lineation, evidenced by the density distribution of the principal axis (K_{max}), is observed in all subsites (Table 2, Supplementary Data Fig. 8), except for Unit I in the outcrop, where an exchange between K_{max} and K_{int} exists, probably related to the low number of samples. These data, coupled with the null correlation of Pj/K_m and the good correspondence of Pj/T (Fig. 9b,c), indicate the low influence of mineralogical changes on the degree of anisotropy and well-preserved flat-lying AMS ellipsoids. The susceptibility axis distribution and the scalar parameters for all the subsites suggest a primary depositional fabric within the range of the usual values for fine-grained deposits (*e.g.*, Tarling and Hrouda, 1993; Hrouda and Chadima, 2019). Likewise, comparison of the blocks and outcrops for each unit indicates a good correspondence of the parameters and eigenvector orientations, corresponding to a common genetic origin of the fabrics.

After establishing reliable AMS values for the whole deposits, only the specimens collected in Unit III, between 30 cm above and below the eggs, are considered for further analysis. The Pj/T diagram reveals that most specimens (~90%) are characterized by oblate ellipsoids with different degrees of anisotropy, although there are a few data with prolate or triaxial ellipsoids (~8%), which exhibit similar ranges of anisotropy (Fig. 10a). On the Flinn diagram (Fig. 10b), the main cluster describes a foliated fabric, and the minor, secondary cluster describes a lineated fabric, both being separated from the point of origin (isotropic fabric). Most of the data belonging to the main cluster are located near the F axis, and the scattered samples in the F domain, together with the position of the secondary cluster in the L domain, indicate that the foliation is stronger than the lineation. This kind of fabric distribution is perfect for applying the q–β diagram (Fig. 10c), defined by Taira (1989) and extended by Novak et al. (2014) and Bradák-Hayashi et al. (2016), which compares the degree of orientation of the particles and sorting (q) with the imbrication of the K_{min} (β). The result is a correlation between the ellipsoid shape, the grain alignments, and the most probable depositional processes. Most of the data present low q-values (<0.2) and normal imbrication angles (5°–25°), indicating the preferential influence of gravity and current processes on particle deposition. A minor contribution from the viscous suspension and grain collision processes is reflected by a subset with q-values from 0.4 to 0.7, whereas the few scattered points above the q-value of 0.7 or > 30° imbrication suggest the limited influence of bioturbation, tectonic strain, or deformations (Fig. 10c).

Stereographic projections of the orientation and density distribution of the magnetic axes show that K_{max} and K_{int} are scattered in the bedding plane, and K_{min} parallel to the bedding pole (Fig. 10d,e). However, the statistics for magnetic lineation (K_{max}) present NNW-SSE orientation close to the horizontal, whereas the K_{max} for individual specimens forms a broad cluster along the NNE-SSW to NW-SE orientations and < 30° plunge (90% of data < 20°). Two maxima appear in the cluster around NNE and NW (Fig. 10e). Both directions are parallel and almost perpendicular to the palaeoflow established from the palaeocurrent indicators in the field (Fig. 3). In addition, the K_{max} axes of the few prolate ellipsoids show small inclination angles (<10°) and are preferentially parallel-aligned to the NNE-SSW and NW-SE orientations.

6.2. Interpretation

In a primary depositional magnetic fabric, phyllosilicates tend to form accumulations with the K_{min} axes (c-crystallographic axes) perpendicular to the bedding, due to the quiet deposition within the water, resulting in oblate mineralogical fabrics (*e.g.*, Ellwood and Whitney, 1980; Tarling and Hrouda, 1993). A current induces tangential forces that control the parallel or perpendicular alignment of the K_{max} axes (a-crystallographic axes) of the grains and the flow direction, forming a current-generated magnetic fabric (*e.g.*, Sagnotti, 2011; Felleti et al., 2016). Thus, a sedimentary magnetic lineation emerges by a clustering of the K_{max} axes depending on the hydrodynamic conditions (Bradák et al., 2020).

The q-β diagram and the magnetic fabric show a good correlation with the particle arrangement and palaeoflow indicators observed in the field and thin sections (Fig. 4). The q-β diagram reflects the distribution expected for floodplain deposits, which were formed by overflow currents. In these environments, the influences of tangential stress (flow-induced) and settling (gravity-induced) interact during the loss of energy of a water flow (Rees and Woodall, 1975; Taira, 1989; Dong et al., 2013; Bradák et al., 2020). The data are grouped around low q-values (<0.4), indicating good sorting and a progressive loss of energy of the current. The low imbrication angles (<10°), in general correlative with upflow tilting, correspond to low-energy currents (<1 cm/s), which is enough energy to imbricate some grains and allow the action of gravity. In these dynamic conditions, some high imbrication angles (>10°), could correspond to peaks of greater energy in the flows (≥1 cm/s) or to an inclination of the depositional surface (>30°). Scattered specimens fall within the category of the viscous suspension and grain collision, which is normal in unconfined flows.

The flow characteristics established through the magnetic properties also fit well with a magnetic fabric formed by NNW- to NNE-flowing unidirectional currents resulting from the overflow and flooding of the channel banks. Thus, the magnetic lineation (NNW) and two small but significant K_{max} clusters, both parallel and perpendicular to the flow direction (NW and NNE), fit well with the imbricated and aligned grains, roughly parallel to the palaeoflow observed in the thin sections (Fig. 4). The K_{max} ranges fall within the possible directions considering the variability of the current in the bed (*e.g.*, Sagnotti, 2011; Novak et al., 2014; Felleti et al., 2016; Bradák et al., 2020). The correlative cluster on the opposite side of the projection could indicate both up-current and down-current imbrication of the grains observed in the thin section (Bradák et al., 2020). The prolate ellipsoids parallel and perpendicular to the direction of the current suggest both an alignment and rolling of the elongate grains. In addition, the scattered K_{max} and K_{int} along the magnetic foliation reflect the deposition of the grains by gravity when the flow lost energy.

Furthermore, several criteria, such as the well-defined flat fabric, the low degree of anisotropy, the magnetic foliation nearly parallel to the bedding, and the magnetic lineation almost perpendicular to the bedding strike, rule out a tectonic overprint

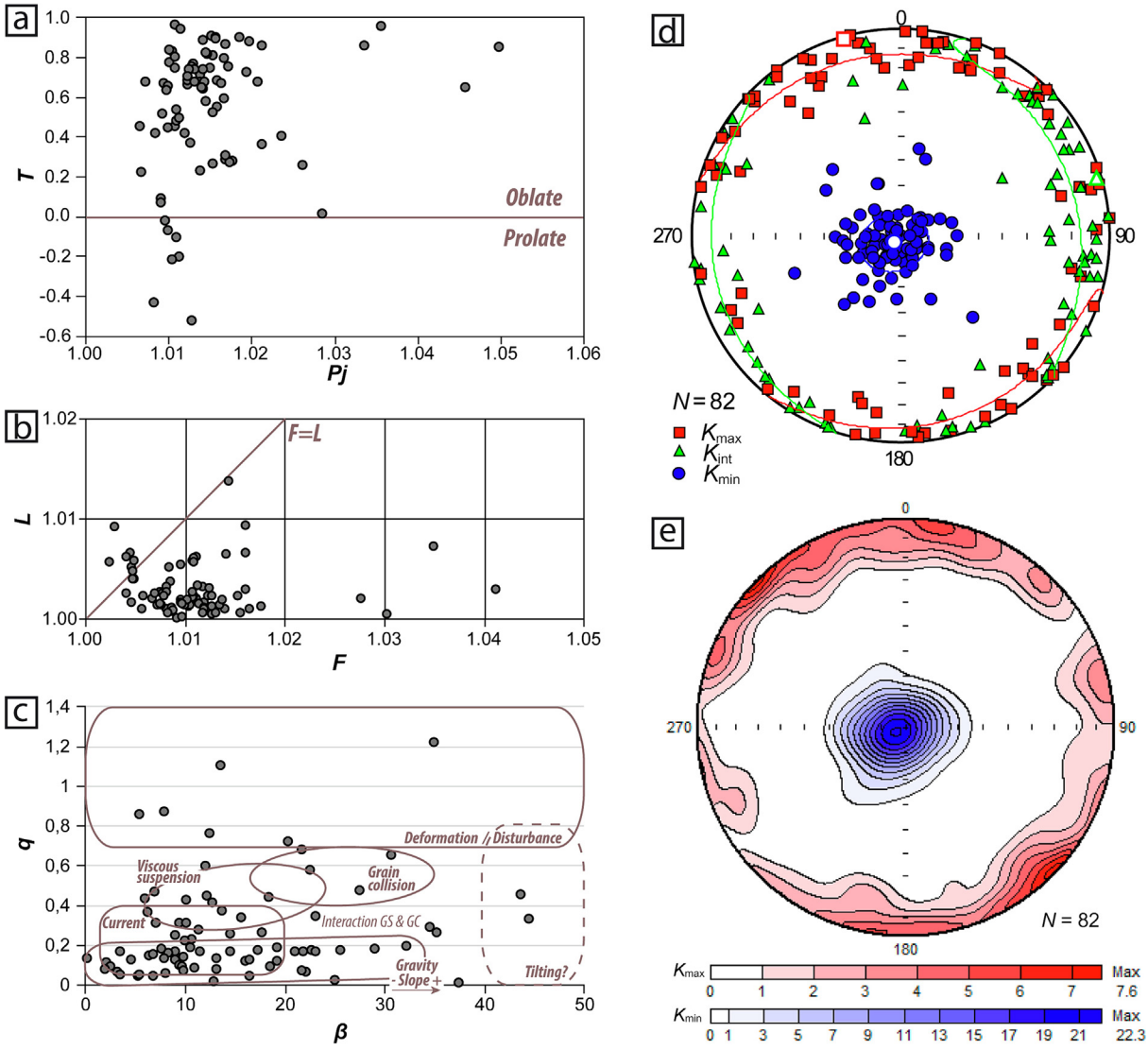

Fig. 10. Graphical plots of the mean magnetic fabric of the Unit III deposits. (a) Jelinek diagram. (b) Flinn diagram. (c) Taira diagram with separate areas related to transportation processes. (d) Equal area projection of the three magnetic axes after restoring bedding to horizontal, including their confidence ellipses. K_{max} in red squares, K_{int} in green triangles and K_{min} in blue circles. The larger symbols indicate the average value for each axis. (e) Contour diagrams with the statistical distribution of magnetic lineations. The red and blue coloured areas represent the directions of K_{max} and K_{min} axis, respectively.

of the magnetic fabric (*e.g.* Cifelli et al., 2015; Hrouda and Chadima, 2019; Stachowska et al., 2020). Moreover, a NE–SW extension direction has been deduced from an AMS analysis of Late Jurassic deposits to the north of the study area (Soto et al., 2012). These authors noted that the tectonic fabric could be related to the influence of the Atouguia da Baleia fault and secondary processes due to regional E–W stretching. Beyond the absence of major faults near Paimogo, the large angle between magnetic lineations and the poor development of the magnetic lineation compared with studies further north suggest a different origin for the magnetic fabric.

These characteristics also allow us to rule out any nesting structure or dinosaur activity since no disrupted fabrics or abrupt changes between egg-bearing materials and the surrounding deposits are observed (see expected fabrics in Supplementary Data Fig. 1). Furthermore, a high degree of anisotropy and *q*-values above 0.8 would be expected as a consequence of the digging and stacking of sediments, similar to the values induced by bioturbation or grain fall in chaotic flows (Novak et al., 2014; Bradák et al., 2020). Conversely, the vertical compaction induced by a dinosaur during the preparation of a ground surface or a mound could be reflected in a planar magnetic fabric. Even then, some disturbances related to the footprints would be expected in accordance with the AMS analysis of dinosaur footprints by García-Lasanta et al. (2013), who established changes in the *Pj* below structures and disruptions toward the footprint boundaries in comparison with the surrounding rocks.

7. On the origin of the Paimogo egg accumulation

Since the excavation of the site, several hypotheses have been postulated to explain the formation of the Paimogo egg accumulation: (1) it is a fossilized nesting ground recording different egg-laying events in a recurrent laying area over different periods of time; (2) it is a single-event deposit, recording the collective nesting behaviour of theropod dinosaurs; or (3) it represents a secondary assemblage caused by the reworking of one or several nests or clutches (Mateus et al., 1997, 1998; Cunha, 2001; Cunha et al., 2004).

The first assumption of our model is the occurrence of a colonial nesting area. Such gregarious behaviour has been inferred in theropods in other sites where clutches have appeared close to one another (*e.g.*, Carpenter, 1999; Tanaka et al., 2019). The results limit the possibilities of the original laying conditions:

- *Several females in one season*. A group of females showing gregarious behaviour met in the nesting area but lived separately, since one group drank freshwater (Group A), and the other more concentrated waters (Group B). The occurrence of several sizes of females can easily be explained.
- *One female over at least three points in time*. The same female used the area at different periods over several breeding seasons. The variations in geochemistry could indicate that the dinosaur consumed water from rivers or evaporated ponds; Group A would represent seasons of wetter conditions, whereas Group B would correspond to drier seasons. The different sizes of the eggs could reflect an increase in the size of the female, possibly a juvenile becoming an adult.
- *Several females in different seasons*. A group of females showing gregarious behaviour lived together, but the varying geochemistry is a result of shifts in the moisture conditions in different years. The occurrence of several sizes of females can easily be explained.

Traditionally, closely grouped and well-preserved eggs, above all when the embryos' bones are associated with the eggs (*e.g.*, Currie and Eberth, 1993; Horner, 1999; Huh and Zelenitsky, 2002; Buffetaut et al., 2005; Grellet-Tinner et al., 2006), have been considered to be clutches and regarded as nests only in the presence of nesting structures. However, more rigorous criteria established by different authors have been considered necessary evidence for defining any egg assemblages as dinosaur nesting structures, including nests and clutches (Varricchio et al., 1999; Chiappe et al., 2004; Vila et al., 2010). Recently, some of these features have proved unsuccessful in structureless and pedogenized deposits, in which palaeosol horizons can be useful to discriminate between clutches or accumulations but also present several limitations (*e.g.*, Jackson et al., 2004; Basilici et al., 2017; Botfalvai et al., 2017).

The Paimogo accumulation comprises a considerable number of complete eggs and a significant number of preserved juvenile bones, even articulated within a single egg. However, there is a lack of evidence of nesting in the egg-bearing material. Although little sediment was removed during the excavation of the blocks, there was no record of any rim or ridge in the surrounding sediments. The sedimentary fabric is the same at macro- or microscopic scale without evidence of a filled, stacked, or truncated sedimentary architecture. The AMS analysis can rule out a cryptostructure obscured by pedogenic processes, indicating a common sedimentary event of the egg-bearing bed. The only difference is related to a shift in the grain-size distribution and the content of organic matter towards the east that runs in parallel with an increase in bioturbation. Overall, the eggs were accumulated at one time and prior to soil development since the altered eggshells tend to show the composition of carbonated nodules, some root traces penetrate the eggs, and green haloes characteristic of reducing conditions developed around the eggs after burial. Thus, there is no evidence for any preparation of the area as a place for incubating or laying eggs, and the Paimogo site corresponds to an egg accumulation produced as a consequence of the remodelling of previous real clutches or nests.

Even though a similar possibility has been postulated before, mainly based on the number of eggs without a clear nesting structure, several incongruencies due to an absence of deep and detailed study made it very speculative (Cunha, 2001). The results of this study have led us to propose a new model that offers an almost complete scenario, as well as discussing the original arrangement of the nesting area and theropod behaviour (Fig. 11). The sequence of events encompasses four simplified stages from the egg-laying until the formation of the accumulation.

During the breeding season, several (at least two, but probably more) dinosaurs and a crocodylomorph laid their eggs in a nesting area located in the dried terrain of an overbank area close to the main channel (<2 km), as indicated by the compound palaeosol profiles (*e.g.*, Marriott and Wright, 1993; Kraus, 1999; Catena et al., 2017). The sedimentary environment and the channel architecture suggest periodic shifts in the water discharge, which may be associated with high seasonality featuring extreme dry and wet periods (Hill, 1988; Martinius and Gowland, 2011; Myers et al., 2012). To prevent embryos from drowning due to the nest flooding, the breeding period would have been restricted to the dry season, when the area was stable as a consequence of low water discharge and streams being confined to their channels (Fig. 11a). The eggs were laid in mounds built with soil and/or vegetation, and remained in these conditions until the last stages of the brooding period, as inferred from the ontogeny of theropod embryos. See Fig. 12.

A drastic increase in water level, possibly ahead of time, at the start of the wet season induced an overflow and flooding of the channel-adjacent zones where the clutches were located. However, the sedimentary features of the Paimogo area indicate that these flood events were often of low magnitude, characterized by widespread overtopping of channel edges rather than localized crevassing. The lack of erosive structures in the whole, the very fine grain size of the sediments, the geometry of the fluvial channels, the floodplain strata and the presence of vegetative barriers indicates a low relief and erosion potential. In general, this kind of event is low-erosive due to the rapid drop in velocity of the spreading flow, and a significant amount of suspended sediment is carried to the floodplain (*e.g.* Allen, 1982; Hill, 1988; Nichols, 2009; Zhao and Wu, 2015). This suggests that a buried nesting strategy was unlikely because the flows had little capacity to erode and rework the subsurface.

The absence of abrasion and the arrangement of the eggs in the accumulation suggest that they were dragged a short distance by a low-energy flow. The increase in bioturbation and organic matter and the shift in flow velocity inferred towards the east point to the presence of vegetation barriers or topographical steps slowing down the eggs. When the eggs were remodelled, the cover was transported until it stopped at the same barrier, a similar process to what is undergone by peat in floodings (Rodríguez-López et al., 2021). The palaeocurrent indicators, at both micro- and macroscale, and the AMS analysis corroborate a flow approaching from the north, inducing a reorientation and rolling of the eggs, whose longitudinal axes are parallel and perpendicular to these directions. The number of eggs belonging to Group A and their random arrangement in the middle of the subsets reflect low displacement, indicating that they were reoriented by floating and a few of them by rolling only. Group B underwent greater transportation, until it was halted next to the Group A eggs, as indicated by the crescent-shaped distribution (Fig. 11c). The differences observed in the geochemical and isotopic composition of the Group B eggs can be explained by the second female or group of females having a slightly different life history from the individual or individuals that laid the Group A eggs. During mobilization, at least one crocodylomorph nest was also affected, incorporating scattered eggs into the accumulation.

There is also no evidence of weathering, which might have indicated that the eggs underwent a long period of subaerial exposure (Jackson et al., 2004). Thus, a rapid burial of the eggs as a consequence of a high amount of suspended material during a waning

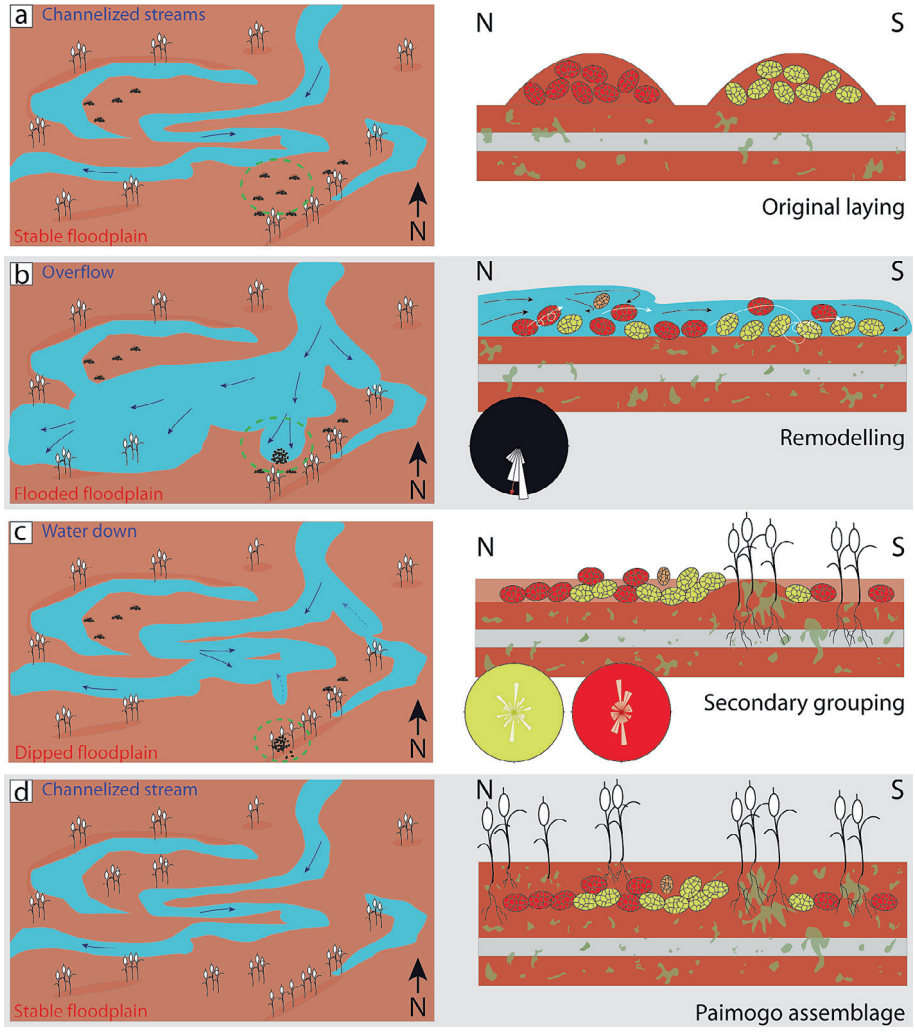

Fig. 11. Sedimentologic evolutionary model for the Paimogo site during the dinosaur laid times. The four sketches represent the key events necessary for the egg accumulation.

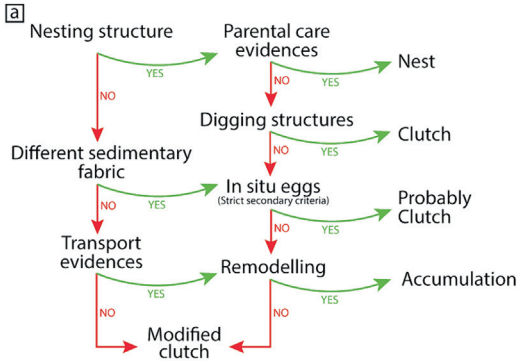

b

	Monogamous clutches	Poligamous clutches	Clutch fidelity	Biostratinomic assemblage
Number of nesting females	one	several	one or more	several
Clutch volume too high for a single laying event	NO	YES	POSSIBLE	POSSIBLE
Eggs show diferential physical features (egg size, eggshell thickness, ornamentation)	NO	POSSIBLE	POSSIBLE	POSSIBLE
Eggs show different geochemical signals	NO	POSSIBLE	MOST LIKELY	MOST LIKELY

Fig. 12. Proposal of an identification key for the recognition of nests, clutches or accumulations. (a) Referred to the observable or physical features of the sediments. (b) Kind of accumulation based on the number and geochemical characteristics of the eggs.

sheet-flood can be inferred. Under a semiarid climate, moderately well-drained conditions subsequently prevailed although the moisture was enough to maintain rooted vegetation (Myers et al., 2012) that could protect the eggs from predators (Fig. 11d).

We favour the hypothesis of colonial nesting versus recurring nesting due to the unlikelihood of nesting mounds being preserved from one season to another. In light of the periodic overflows that affected the Paimogo area and the nesting strategy of theropods, the remodelling of multi-seasonal clutches seems less probable. As mentioned above, mounds covered with plants were the most probable nesting structure, but these were not very robust in the face of extreme processes. Abandoned mound clutches between laying seasons would thus be destroyed during the floodings that occurred during the wet season of the same year. In addition, the

vulnerability of unattended nesting mounds over long periods of time would facilitate predation/scavenging on unsuccessful nests.

Having taken into account the challenges proposed by Basilici et al. (2017) and our own throughout this study, we therefore propose some criteria that could improve the distinction between nests, clutches, and accumulations in structureless deposits, in accordance with the criteria previously proposed by Chiappe et al. (2004), Varricchio et al. (1999), and Vila et al. (2010). We highlight the possibility of characterizing uncertainties associated with the origin of the eggs in an accumulation (Fig. 12). Nevertheless, it is beyond question that the amount of proxies used in this work cannot be applied in all taphonomic studies.

8. Conclusions

Our analysis of the systematic palaeontology, taphonomy, sedimentology, anisotropy of magnetic susceptibility, and geochemistry of the Paimogo egg assemblage has revealed that the accumulation had a more complex origin than previously reported.

At least two species, an undetermined allosauroid and an undetermined crocodylomorph, nested in the overbank deposits of a fluvial channel.

The Paimogo egg assemblage represents a secondary deposit of complete eggs after a flooding event in the fluvial plain. The accumulation resulted from the dismantling of several allosaur dinosaur and crocodylomorph clutches, belonging to a minimum of one crocodile female and two dinosaur females, or to a single female laying eggs in different seasons.

Our reviewed calculations of water vapour conductance and analysis of the sedimentological evidence support the notion that the allosauroids buried their eggs to preserve adequate incubation conditions. The relatively low energy of the current generating the deposit was not able to break the eggs, and it is unlikely that it was able to remove the eggs from excavated nests, which supports the idea of a mound nesting strategy both for Jurassic crocodylomorphs and allosauroids.

The use of anisotropy of magnetic susceptibility allowed us to rule out a cryptostructure obscured by pedogenic processes and proved to be a convenient tool for studying nesting structures.

Multidisciplinary approaches, including taphonomic, sedimentological, and geochemical analyses, are needed to be able to evaluate egg assemblages correctly before making assumptions on the palaeoecology of extinct species.

CRediT authorship contribution statement

L. Ezquerro: Conceptualization, Data curation, Investigation, Methodology, Supervision, Writing – original draft, Writing – review & editing. **R. Coimbra:** Data curation, Investigation, Methodology, Writing – original draft, Writing – review & editing. **B. Baulúz:** Data curation, Investigation, Methodology, Writing – original draft, Writing – review & editing. **C. Núñez-Lahuerta:** Data curation, Investigation, Methodology, Writing – original draft, Writing – review & editing. **T. Román-Berdiel:** Data curation, Investigation, Methodology, Writing – original draft, Writing – review & editing. **M. Moreno-Azanza:** Data curation, Investigation, Methodology, Writing – original draft, Writing – review & editing.

Declaration of competing interest

The authors declare that they have no known competing financial interests or personal relationships that could have appeared to influence the work reported in this paper.

Acknowledgements

This work was supported the PLEC2021-008203 project and RYC2021-034473-I, funded by MCIN/AEI/10.13039/501100011033 and by the European Union "NextGenerationEU"/PRTR"; Fundação para a Ciência e Tecnologia (FCT-MCTES) of Portugal (projects PTDC/CTA-PAL/31656/2017 and PTDC/CTA-PAL/2217/2021), and Research Unit GeoBioTec UIDB/04035/2020. Also, the work is part of the Carmen Nunez-Lahuerta is supported by FJC2020-044561-I-; MCIN, co-financed by the NextGeneration EU/PRTR.

Appendix A. Supplementary data

Supplementary data to this article can be found online at https://doi.org/10.1016/j.gsf.2024.101872.

References

Allen, J.R.L., 1982. Sedimentary Structures: Their Character and Physical Basis. Elsevier, New York, Vol. I & II.
Alves, T.M., Gawthorpe, R.L., Hunt, D.H., Monteiro, J.H., 2002. Jurassic tectono-sedimentary evolution of the northern Lusitanian basin (offshore Portugal). Marine Petroleum Geology 19, 727–754.
Antunes, M.T., Taquet, P., Ribeiro, V., 1998. Upper Jurassic dinosaur and crocodile eggs from Paimogo nesting site (Lourinha-Portugal). Memorias Da Academia De Ciencias De Lisboa 37, 83–100.
Ar, A., Rahn, H., 1985. Pores in avian eggshells: gas conductance, gas exchange and embryonic growth rate. Respir Physiol 61 (1), 1–20.
Basilici, G., Hechenleitner, E.M., Fiorelli, L.E., Bó, P.F., Mountney, N.P., 2017. Preservation of titanosaur egg clutches in Upper Cretaceous cumulative palaeosols (Los Llanos Formation, La Rioja, Argentina). Palaeogeog. Palaeoclimatol. Palaeoecol. 482, 83–102.
Birkeland, P.W., 1999. Soils and Geomorphology. Oxford University Press, New York, USA.
Borradaile, G.J., Henry, B., 1997. Tectonic applications of magnetic susceptibility and its anisotropy. Earth Sci. Rev. 42, 49–93.
Botfalvai, G., Csiki-Sava, Z., Grigorescu, D., Vasile, S., 2017. Taphonomical and palaeoecological investigation of the late cretaceous (Maastrichtian) Tuștea vertebrate assemblage (Romania; Hațeg Basin) - insights into a unique dinosaur nesting locality. Palaeogeog. Palaeoclimatol. Palaeoecol. 468, 228–262.
Bradák, B., Seto, Y., Chadima, M., Kovács, J., Tanos, P., Újvári, G., Hyodo, M., 2020. Magnetic fabric of loess and its significance in Pleistocene environment reconstructions. Earth Sci. Rev. 210, 103385.
Bradák-Hayashi, B., Biro, T., Horvath, E., Vegh, T., Csillag, G., 2016. New aspects of the interpretation of the loess magnetic fabric, Cerna Valley succession. Hungary. Quat. Res. 86, 348–358.
Brookfield, M.E., 2004. Principles of Stratigraphy. Blackwell Publishing Ltd.
Buffetaut, E., Grellet-Tinner, G., Suteethorn, V., Cuny, G., Tong, H., Košir, A., Cavin, L., Chitsing, S., Griffiths, P.J., Tabouelle, J., Le Loeuff, J., 2005. Minute theropod eggs and embryo from the Lower Cretaceous of Thailand and the dinosaur–bird transition. Naturwissenschaften 92, 477–482.
Buol, S.W., Southard, R.J., Graham, R.C., McDaniel, O.A., 2011. Soil Genesis and Classification. Wiley-Blackwell, Oxford.
Carpenter, K., 1999. Eggs, Nests, and Baby Dinosaurs: A Look at Dinosaur Reproduction. Indiana University Press, Bloomington, IN, USA.
Carrano, M., Mateus, O., Mitchell, J., 2013. First definitive association between embryonic allosaurus bones and Prismatoolithus eggs in the Morrison Fm. (Upper Jurassic, Wyoming, USA). Society of vertebrate paleontology, Abstracts of papers 73rd Annual meeting, 101A.
Carvalho, J., Matias, L., Torres, L., Manupella, G., Pereira, R., Victor, L.M., 2005. The structural and sedimentary evolution of the Arruda and Lower Tagus sub-basins, Portugal. Marine Petroleum Geology 22, 427–453.
Catena, A., Hembree, D., Saylor, B., Anaya, F., Croft, D., 2017. Paleosol and ichnofossil evidence for significant Neotropical habitat variation during the late middle Miocene (Serravallian). Palaeogeog. Palaeoclimatol. Palaeoecol. 487, 381–398.
Chadima, M., Jelinek, V., 2009. Anisoft 4.2: Anisotropy Data Browser for Windows, Agico, Inc.
Chadima, M., Hrouda, F., Melichar, R., 2006. Magnetic fabric study of the SE Rhenohercynian Zone (Bohemian Massif): implications for dynamics of the Paleozoic accretionary wedge. Tectonophysics 418, 93–109.
Chadima, M., Hrouda, F., 2009. Cureval 8.0: Thermomagnetic Curve Browser for Windows. Agico Inc..
Cheong-Bin, K., Ihsan, A., Fereydoun, G., Ho, C., 2009. Stable isotopic composition of dinosaur eggshells and pedogenic carbonates in the upper cretaceous seonso formation, South Korea: Paleoenvironmental and diagenetic implications. Cretaceous Res. 30, 93–99.
Chiappe, L.M., Schmitt, J.G., Jackson, F.D., Garrido, A., Dingus, L., Grellet-Tinner, G., 2004. Nest structure for sauropods: sedimentary criteria for recognition of dinosaur-nesting traces. PALAIOS 19, 89–95.

Cifelli, F., Mattei, M., Chadima, M., Lenser, S., Hirt, A.M., 2009. The magnetic fabric in "undeformed clays": AMS and neutron texture analyses from the Rif Chain (Morocco). Tectonophysics 466, 79–88.
Cifelli, F., Ballato, P., Alimohammadian, H., Sabouri, J., Mattei, M., 2015. Tectonic magnetic lineation and oroclinal bending of the Alborz range: implications on the Iran-Southern Caspian geodynamics. Tectonics 34, 116–132.
Coimbra, C., Moreno-Azanza, M., Ezquerro, L., Nuñez-Lahuerta, C., Gasca, J.M., Immenhauser, A., Mateus, O., Rocha, F., 2023. Evaluating and comparing geochemical sampling protocols in dinosaur eggshells: refining Cretaceous ecosystem research. Cretaceous Res. 151, 105632.
Cojan, I., Renard, M., Emmanuel, L., 2003. Palaeoenvironmental reconstruction of dinosaur nesting sites based on a geochemical approach to eggshells and associated palaeosols (Maastrichtian, Provence Basin, France). Palaeogeog. Palaeoclimatol. Palaeoecol. 191, 118–138.
Collinson, J., Mountney, N., Thompson, D., 2006. Sedimentary Structures. Terra Publishing, London.
Cunha, P., 2001. A sedimentologia da jazida de ovos (ninhos de dinossauros e crocodilos) de Paimogo (Kimeridgiano terminal-Titoniano basal. Unpublished report, Lourinhá - Portugal).
Cunha, P.P., Mateus, O., Antunes, M.T., 2004. The sedimentology of the Paimogo dinosaur nest site (Portugal, Upper Jurassic). 23rd IAS Meet., Abstr. Book, Coimbra, 93.
Currie, P.J., Eberth, D.A., 1993. Palaeontology, sedimentology and palaeoecology of the Iren Dabasu Formation (Upper Cretaceous), Inner Mongolia. People's Republic of China. Cretaceous Res. 14, 127–144.
Daniels, J.M., 2003. Floodplain aggradation and pedogenesis in a semiarid environment. Geomorphology 56, 225–242.
Dawson, R.R., Field, D.J., Hull, P.M., Zelenitsky, D.K., Therrien, F., Affek, H.P., 2020. Eggshell geochemistry reveals ancestral metabolic thermal regulation in Dinosauria. Sci. Adv. 6 (7), eaax9361. https://doi.org/10.1126/sciadv.aax9361.
Deeming, D.C., 2006. Ultrastructural and functional morphology of eggshells supports idea that dinosaur eggs were incubated buried in a substrate. Paleontology 49, 171–185.
Deeming, D.C., Ferguson, M.W.J., 1991. Egg Incubation: Its Effects on Embryonic Development in Birds and Reptiles. Cambridge University Press, p. 462.
Domingo, L., Barroso-Barcenilla, F., Cambra-Moo, O., 2013. Paleoenvironmental reconstruction of the "Lo Hueco" Fossil Site (Upper Cretaceous, Cuenca, Spain): Preliminary stable isotope analyses on crocodilians and dinosaurs. PALAIOS 28, 195–202.
Dong, Z.-M., Currie, P.J., 1996. On the discovery of an oviraptorid skeleton on a nest of eggs at Bayan Mandahu, Inner Mongolia, People's Republic of China. Can. J. Earth Sci. 33, 631–636.
Dong, J., Gao, R., Wang, Y., Zhang, S., Yao, P., Chi, Z., Zhao, Z., 2013. Magnetic fabric study of Late Holocene sediments in Huangqihai Lake, Inner Mongolia and its sedimentary significance. Acta Geol. Sin. 87 (1), 186–196.
Ellwood, B.B., Whitney, J.A., 1980. Magnetic fabric of the Elberton granite, Northeast Georgia. J. Geophys. Res. 85, 1481–1486.
Erben, H.K., Hoefs, J., Wedepohl, K.H., 1979. Paleobiological and isotopic studies of eggshells from a declining dinosaur species. Paleobiology 5, 380–414.
Felleti, F., Dall'Olio, E., Muttoni, G., 2016. Determining flow directions in turbidites: an integrated sedimentological and magnetic fabric study of the Miocene Marnoso Arenacea Formation (northern Apennines, Italy). Sediment. Geol. 335, 197–215.
Fernandes, A., Mateus, O., Balauz, B., Coimbra, R., Ezquerro, L., Núñez-Lahuerta, C., Suteu, C., Moreno-Azanza, M., 2021. The Paimogo dinosaur egg clutch revisited: using one of Portugal's most notable fossils to exhibit the scientific method. Geoheritage 13, 66.
García-Lasanta, C., Oliva-Urcia, B., Román-Berdiel, T., Casas, A.M., Pérez-Lorente, F., 2013. Development of magnetic fabric in sedimentary rocks: insights from early compactional structures. Geophys. J. Int. 194, 182–199.
Grellet-Tinner, G., Chiappe, L., Norell, M., Bottjer, D., 2006. Dinosaur eggs and nesting behaviors: a paleobiological investigation. Palaeogeogr. Palaeoclimatol. Palaeoecol. 232, 294–321.
Grellet-Tinner, G., Fiorelli, L.E., 2010. A new Argentinean nesting site showing neosauropod dinosaur reproduction in a Cretaceous hydrothermal environment. Nat. Commun. 1, 32.
Grellet-Tinner, G., Fiorelli, L.E., Salvador, R.B., 2012. Water vapor conductance of the lower Cretaceous dinosaurian eggs from Sanagasta, La Rioja, Argentina: paleobiological and paleoecological implications for South American faveoloolithid and megaloolithid eggs. PALAIOS 30, 207–223.
Grigorescu, D., Garcia, G., Csiki, Z., Codrea, V., Bojar, A.V., 2010. Uppermost Cretaceous megaloolithid eggs from the Haţeg Basin, Romania, associated with hadrosaur hatchlings: search for explanation. Palaeogeog. Palaeoclimatol. Palaeoecol. 293, 360–374.
Hechenleitner, E.M., Fiorelli, L.E., Grellet-Tinner, G., Leuzinger, L., Basilici, G., Taborda, J.A., de la Vega, S.R., Bustamante, C.A., 2016. A new Upper Cretaceous titanosaur nesting site from La Rioja (NW Argentina) with implications for titanosaur nesting strategies. Palaeontology 59, 1–14.
Hill, G., 1988. The sedimentology and lithostratigraphy of the Upper Jurassic Lourinha formation, Lusitanian Basin, Portugal. Ph.D. thesis. Open University, London (unpublished).
Hogan, J.D., Varricchio, D.J., 2023. Chthonic severance: dinosaur eggs of the Mesozoic, the significance of partially buried eggs and contact incubation precursors. Phil. Trans. R. Soc. B, 37820220144.
Hirsch, K.F., 1994. Upper Jurassic eggshells from western interior of North America. In: Carpenter, K., Hirsch, K., Horner, J.R. (Eds.), Eggs and Babies. Cambridge University Press, Cambridge, pp. 137–150.
Horner, J.R., 1999. Egg clutches and embryos of two Hadrosaurian dinosaurs. J. Vertebr. Paleontol. 19, 607–611.
Horner, J.R., 2000. Dinosaour reproduction and parenting. Annu. Rev. Earth Planet. Sci. 28, 19–45.
Horner, J.R., Makela, R., 1979. Nest of juveniles provides evidence of family structure among dinosaurs. Nature 282, 296–298.
Hrouda, F., 1982. Magnetic anisotropy of rocks and its application in geology and geophysics. Geophys. Surv. 5, 37–82.
Hrouda, F., Chadima, M., 2019. Examples of tectonic overprints of magnetic fabrics in rocks of the Bohemian Massif and Western Carpathians. Int. J. Earth Sci. 109, 1–16.
Huh, M., Zelenitsky, D.K., 2002. Rich dinosaur nesting site from the Cretaceous of Bosung County, Chullanam-do Province, South Korea. J. Vertebr. Paleontol. 22, 716–718.
Jackson, F.D., Garrido, A., Schmitt, J.G., Chiappe, L., Dingus, L., Loope, D., 2004. Abnormal, multilayered titanosaur (Dinosauria: Sauropoda) eggs from in situ clutches at the Auca Mahuevo locality, Nuequén Province Argentina. J. Vertebr. Paleontol. 24, 913–922.
Jackson, F.D., Varricchio, D.J., Jackson, R.A., Walde, A., Bishop, G., 2015. Taphonomy of extant desert tortoise and loggerhead sea turtle nesting sites: implications for interpreting the fossil record. PALAIOS 30, 207–223.
Jackson, F.D., Varricchio, D.J., 2016. Fossil egg and eggshells from the Upper Cretaceous Hell Creek Formation. Montana. J. Vertebr. Paleontol. 36, e1185432.
Jelinek, V., 1981. Characterization of the magnetic fabric of rocks. Tectonophysics 79, 63–70.
Kim, S., Hwang, I.G., Ghim, Y.S., Kim, N.-H., Lee, Y.-N., 2022. Upper Cretaceous (Coniacian-Santonian) dinosaur nesting colony preserved in abandoned crevasse splay deposits Wi Island, South Korea. Palaeogeogr. Palaeoclimatol., Palaeoecol. 585 (1), 110728. https://doi.org/10.1016/j.palaeo.2021.110728.
Kraus, M.J., 1999. Palaeosols in clastic sedimentary rocks: their geologic applications. Earth Sci. Rev. 47, 41–70.
Kraus, J.M., Alsan, A., 1993. Eocene hydromorphic paleosols: significance for interpreting ancient floodplain processes. J. Sediment. Petrol. 63, 453–463.
Kraus, M.J., Hasiotis, S.T., 2006. Significance of different modes of rhizolith preservation to interpreting. Palaeoenvironmental and palaeohydrologic settings: examples from Palaeogene palaeosols, Bighorn Basin, Wyoming, U.S. A. J. Sediment. Res. 76, 633–646.
Kullberg, J.C., 2000. Evolução tectónica mesozóica da Bacia Lusitaniana. PhD Thesis. Univ. Nova Lisboa, 361 p. https://run.unl.pt/handle/10362/1465.
Laskar, A.H., Mohabey, D., Bhattacharya, S.K., Liang, M., 2020. Variable thermoregulation of Late Cretaceous dinosaurs inferred by clumped isotope analysis of fossilized eggshell carbonates. Heliyon 6, e05265.
Leinfelder, R.R., Wilson, R.C.L., 1989. Seismic and sedimentologic features of Oxfordian-Kimmeridgian syn-rift sediments on the eastern margin of the Lusitanian Basin. Geol. Rundschau 78, 81–104.
Liang, X., Wan, S., Yang, D., Zhou, S., Wu, S., 2009. Dinosaur eggs and dinosaur egg-bearing deposits (Upper Cretaceous) of Henan Province, China: Occurrences, palaeoenvironments, taphonomy and preservation. Prog. Nat. Sci. 19, 1587–1601.
Lucas, S., Tanner, L., 2021. Late Pennsylvanian calcareous paleosols from central New Mexico: implications for paleoclimate. New Mex. Geol. 43, 3–9.
Machette, N.M., 1985. Calcic soils of the southwestern United States. In: Weide, D.L. (Ed.), Soils and Quaternary Geology of the Southwestern United States. Geological Society of America, Special Paper 203, pp. 10–21.
Mack, G.H., James, W.C., Monger, H.C., 1993. Classification of palaeosols. Geol. Soc. Am. Bull. 105, 129–136.
Malafaia, E., Mocho, P., Escaso, F., Ortega, F., 2020. A new carcharodontosaurian theropod from the Lusitanian Basin: evidence of allosauroid sympatry in the European Late Jurassic. J. Vertebr. Paleontol. 40, e1768106.
Marriott, S.B., Wright, V.P., 1993. Palaeosols as indicators of geomorphic stability in two Old Red Sandstone alluvial suites, South Wales. J. Geol. Soc. Lond. 150, 1109–1120.
Martinius, A.W., Gowland, S., 2011. Tide-influenced fluvial bedforms and tidal bore deposits (Late Jurassic Lourinhã Formation, Lusitanian Basin, Western Portugal). Sedimentology 58, 285–324.
Mateus, I., Mateus, H., Antunes, M. T., Mateus, O., Taquet, P., Ribeiro, V., Manuppella, G., 1998. Upper Jurassic theropod dinosaur embryos from Lourinhã (Portugal). In: Antunes, M.T. (Ed.), Upper Jurassic palaeoenvironments in Portugal. Memórias da Academia de Ciências de Lisboa 37, 101-110.
Mateus, I., Mateus, H., Antunes, M.T., Mateus, O., Taquet, P., Ribeiro, V., Manuppella, G., 1997. Couvée, oeufs et embryons d'un Dinosaure Théropode du Jurassique superieur de Lourinhã (Portugal). C.R. Académie Des Sciences, Sciences De La Terre Et Des Planètes, Paris 325, 71–78.
Mateus, O., Walen, A., Antunes, M.T., 2006. The large theropod fauna of the Lourinha Formation (Portugal) and its similarity to that of the Morrison Formation with a description of a new species of Allosaurus. Paleontology and Geology of the Upper Jurassic Morrison Formation: Bulletin 36, 123.
Mateus, O., Antunes, M.T., Taquet, P., 2001. Dinosaur ontogeny: the case of Lourinhanosaurus (Late Jurassic, Portugal). J. Vertebr. Paleontol. 21, 78.
Mateus, O., Dinis, J., Cunha, P., 2017. The Lourinhã Formation: the Upper Jurassic to lower most Cretaceous of the Lusitanian Basin, Portugal – landscapes where dinosaurs walked. Ciências Da Terra 19, 75–97.

Moretti, M., Soria, J.M., Alfaro, P., Walsh, N., 2001. Asymmetrical soft-sediment deformation structures triggered by rapid sedimentation in turbiditic deposits (Late Miocene, Guadix Basin, Southern Spain). Facies 44, 283–294.
Morrison, R.B., 1964. Soil stratigraphy: principles, applications *to* differentiation *and* correlation *of* quaternary deposits *and* landforms, *and* applications *to* soil science. PhD Thesis, Univ. of Nevada (Unpublished).
Myers, T.S., Tabor, N.J., Jacobs, L.L., Mateus, O., 2012. Palaeoclimate of the Late Jurassic of Portugal: comparison with the western United States. Sedimentology 59, 1695–1717.
Nichols, G., 2009. Sedimentology and Stratigraphy. Wiley-Blackwell, New-York.
Norell, M.A., Clark, J.M., Chiappe, L.M., Dashzeveg, D., 1995. A nesting dinosaur. Nature 378, 774–776.
Novak, B., Housen, B., Kitamura, Y., Kanamatsuc, T., Kawamura, K., 2014. Magnetic fabric analyses as a method for determining sediment transport and deposition in deep sea sediments. Mar. Geol. 356, 19–30.
Oser, S., Jackson, F., 2014. Sediment and eggshell interactions: using abrasion to assess transport in fossil eggshell accumulations. Hist. Biol. 26 (2), 165–172. https://doi.org/10.1080/08912963.2013.814650.
Owen, G., 1987. Deformation processes in unconsolidated sands. In: Deformation of sediments and sedimentary rocks. Eds. Jones, M.E., Preston, R.M.F. Geological Society Spec. Publ. 29. 11-24.
Paganelli, C.V., Olszowka, A., Ar, A., 1974. The avian eggs: Surface area, volume and density. Condor 76, 319–325.
Park, M.E., Cho, H., Son, M., Sohn, Y.K., 2013. Depositional processes, paleoflow patterns, and evolution of a Miocene gravelly fan-delta system in SE Korea a constrained by anisotropy of magnetic susceptibility analysis of interbedded mudrocks. Mar. Pet. Geol. 48, 206–223.
Pietucowski, G., 1998. Dinosaur nesting ground from the Early Jurassic fluvial deposits, Holy Cross Mountains (Poland). Geological Quarterly 42, 461–476.
Pueyo Anchuela, O., Ramajo, J., Gil Imaz, A., Meléndez, G., 2013. Analysis of anisotropy of magnetic susceptibility in iron-oolitic beds: a potential tool for paleocurrent identification. Int. J. Earth Sci. (geol Rundsch) 102, 1131–1149.
Rasmussen, E.S., Lomholt, S., Andersen, C., Vejbæk, O.V., 1998. Aspects of the structural evolution of the Lusitanian Basin in Portugal and the shelf and slope area offshore Portugal. Tectonophysics 300, 199–225.
Rees, A.I., Woodall, W.A., 1975. The magnetic fabric of some laboratory-deposited sediments. Earth Planet. Sci. Lett. 25, 121–130.
Rees, A.I., Brown, C.M., Hailwood, E.A., Riddy, P.J., 1982. Magnetic fabric of bioturbated sediment from the northern Rockall Trough: comparison with modern currents. Mar. Geol. 46, 161–173.
Retallack, G., 1988. Field recognition of paleosols. Geol. Soc. Am. Spec. Pap. 216, 1–19.
Ricqlès, A., Mateus, O., Antunes, M.T., Taquet, P., 2001. Histomorphogenesis of embryos of Upper Jurassic Theropods from Lourinha (Portugal). Comptes Rendus De L Academie Des Sciences Serie Ii Fascicule a-Sciences De La Terre Et. Des Planetes 332, 647–656.
Riera, V., Anadón, P., Oms, O., Estrada, R., Maestro, E., 2013. Dinosaur eggshell isotope geochemistry as tools of palaeoenvironmental reconstruction for the Upper Cretaceous from the Tremp Formation (Southern Pyrenees). Sediment. Geol. 294, 356–370.
Rochette, P., Jackson, M., Aubourg, C., 1992. Rock magnetism and the interpretation of anisotropy of magnetic susceptibility. Rev. Geophys. 30, 209–226.
Rodríguez-López, J., Soria, A., Liesa, C., 2021. Extreme-flood-related peat blocks: an anthropocene analogue to ancient coal-forming environments. J. Sediment. Res. 91, 243–261.
Sabath, K., 1991. Upper Cretaceous amniotic eggs from the gobi desert. Acta Paleontol. Pol. 36, 151–192.
Sagnotti, L., 2011. Magnetic Anisotropy. In: Gupta, H.K. (Ed.), Encyclopedia of Solid Earth Geophysics. Springer, Dordrecht.
Sander, PM, Peitz, C, Jackson, FD, Chiappe, LM., 2008. Upper Cretaceous titanosaur nesting sites and their implications for sauropod dinosaur reproductive biology. Palaeontogr Abt. A 284, 69–107.
Sarkar, A., Bhattacharya, S.K., Mohabey, D.M., 1991. Stable-isotope analyses of dinosaur eggshells: paleoenvironmental implications. Geology 19, 1068–1071.
Schneider, C.A., Rasband, W.S., Eliceiri, K.W., 2012. NIH Image to ImageJ: 25 years of image analysis. Nat. Methods 9, 671–675.
Selley, R.C., 2000. Applied Sedimentology. Academic Press.
Seymour, R.S., 1979. Dinosaur eggs: gas conductance through the shell, water loss during incubation and clutch size. Paleobiology 5, 1–11.
Soil Survey Staff, 2010. Keys to Soil Taxonomy, 11th. USDA Natural Resources Conservation Service, Washington, DC, USA.
Soto, R., Kullberg, J., Oliva-Urcia, B., Casas-Sainz, A., Villalaín, J.J., 2012. Switch of Mesozoic extensional tectonic style in the Lusitanian basin (Portugal): Insights from magnetic fabrics. Tectonophysics 536, 122–135.
Stachowska, A., Łoziński, M., Śmigielski, M., Wysocka, A., Jankowski, L., Ziółkowski, P., 2020. Anisotropy of magnetic susceptibility as an indicator for palaeocurrent analysis in folded turbidites (Outer Western Carpathians, Poland). Sedimentology 67, 3783–3808.
Syvitski, J.P.M., 1991. Principles, Methods, and Application of Particle Size Analysis. Cambridge University Press, New York.
Taira, A., 1989. Magnetic fabrics and depositional processes. In: Taira, A., Masuda, F. (Eds.), Sedimentary Facies in the Active Plate Margin. Terra Scientific Publishing Company, Tokyo, pp. 43–77.
Tanaka, K., Zelenitsky, D.K., Therrien, F., Kobayashi, Y., 2018. Nest substrate reflects incubation style in extant archosaurs with implications for dinosaur nesting habits. Sci. Rep. 8, 3170. https:// doi .org /10 .1038 /s41598 -018 -21386 –x.
Tanaka, K., Zelenitsky, D.K., Therrien, F., 2015. Eggshell porosity provides insight on evolution of nesting in dinosaurs. PLoS One 10 (11), e0142829.
Tanaka, K., Kobayashi, Y., Zelenitsky, D., Therrien, F., Lee, Y., Barsbold, R., Kubota, K., Lee, H., Chinzorig, T., Damdinsuren, I., 2019. Exceptional preservation of a Late Cretaceous dinosaur nesting site from Mongolia reveals colonial nesting behavior in a non-avian theropod. Geology 47, 843–847.
Tarling, D.H., Hrouda, F., 1993. The Magnetic Anisotropy of Rocks. Chapman & Hall, London.
Taylor, A.M., Gowland, S., Leary, S., Keogh, K.J., Martinius, A.W., 2014. Stratigraphical correlation of the Late Jurassic Lourinhã Formation in the Consolacão Subbasin (Lusitanian Basin) Portugal. Geol. J. 49, 143–162.
Varricchio, D.J., Jackson, F., Borkowski, J.J., Trueman, C.N., 1999. A nesting trace with eggs for the Cretaceous theropod dinosaur Troodon formosus. J. Vertebr. Paleontol. 19, 91–100.
Vila, B., Jackson, F.D., Fortuny, J., Sellés, A.G., Galobart, A., 2010. 3-D modelling of megaloolithid clutches: insights about nest construction and dinosaur behaviour. PLoS One 5, e10362.
Vollmer, F.W., 2018. Automatic contouring of geologic fabric and finite strain data on the unit hyperboloid. Comput. Geosci. 115, 134–142. https://doi.org/10.1016/j.cageo.2018.03.006.
Waldhausl, P., Ogleby, C., 1994. 3x3-Rules for simple photogrammetric documentation of architecture. In: Proceedings of the Symposium of the ISPRS Commission V Close Range Techniques and Machine Vision. The International Archives of the Photogrammetry, Remote Sensing and Spatial Information Sciences,, pp. 426–429.
Wilson, R.C.L., Hiscott, R.N., Willis, M.G., Gradstein, F.M., 1989. The Lusitanian Basin of West-Central Portugal: Mesozoic and Tertiary tectonic, stratigraphic, and subsidence History. In: Tankard, A.J., Balkwill, H.R. (Eds.), Extensional Tectonics and Stratigraphy of the North Atlantic margins. AAPG Mem. 46, 341–361.
Yang, T.R., Engler, T., Lallensack, J.N., Samathi, A., Makowska, M., Schillinger, B., 2019. Hatching asynchrony in oviraptorid dinosaurs sheds light on their unique nesting biology. Integr. Org. Biol. 1 (1), obz030.
Zelenitsky, D.K., 2006. Reproductive traits of non-avian theropods. J. Paleont. Soc. Korea 22, 209–216.
Zelenitsky, D.K., Therrien, F., 2008. Phylogenetic analysis of reproductive traits of Maniraptoran theropods and its implications for egg parataxonomy. Paleontology 51 (4), 807–816.
Zhao, L., Wu, F., 2015. Simulation of runoff hydrograph on soil surfaces with different microtopography using a travel time method at the plot scale. PLoS One 10, e0130794.